BNL-104685-2014-TECH

AGS/AD/Tech Note No. 267;BNL-104685-2014-IR

A Proposal to Use a Laser Based Detection System in the AGS for Beam Diagnostics

W. Schaffer

November 1986

Collider Accelerator Department

Brookhaven National Laboratory

U.S. Department of Energy

USDOE Office of Science (SC)

DISCLAIMER

Accelerator Division
Alternating Gradient Synchrotron Department
BROOKHAVEN NATIONAL LABORATORY
Associated Universities, Inc.
Upton, New York 11973

Accelerator Division
Technical Note

AGS/AD/Tech. Note No. 267

A Proposal to Use a Laser Based Detection System in the AGS for Beam Diagnostics

November 6, 1986

W. Schaffer*

Summary

The feasibility of using a laser-based system for beam diagnostics in the Alternating Gradient Synchrotron (AGS) has been studied from first principles. The collision cross-section for a photon-proton collision can be found using the Klein-Nishina formula. The details of this solution are given in Appendix I. After performing the appropriate Lorentz transformations to account for the relativistic speed of the proton, we find that the largest cross-section is obtained if the photon approaches anti-parallel (or parallel) to the proton's path. In this case, the cross-section per unit solid angle is

$$\frac{d\sigma}{d\Omega} = 2.1 \times 10^{-29} \text{ cm}^2/\text{proton}.$$

The collision cross-section is considered to be the effective target area per proton. At maximum capacity there are 1.25×10^{12} protons in an AGS bunch in a volume approximately 900 cm by 0.2 cm by 0.3 cm. The total effective target area for an anti-parallel approach is found to be

$$\left(\frac{d\sigma}{d\Omega}\right)_{TOT} = 4.3 \times 10^{-16} \text{ cm}^2.$$

See Appendix I for details.

---

*Summer student.

Due to the relativistic speed of the protons, the incident photons undergo a double Doppler shift in frequency. Appendix II studies this aspect of the physics in detail. In Appendix III, the specifics of a few of the commercially available lasers are studied. The number and the frequency of the scattered photons for different scattering angles is calculated for three different approaches: parallel, anti-parallel, and perpendicular to the path of the beam. (The parallel approach is discarded as a possibility because the photons are not scattered into the visible range, a prerequisite for imaging. The perpendicular approach has a significantly smaller scattering cross-section.) The YAG and CO2 lasers appear most promising. The YAG scatters 5,800 photons while the CO2 scatters 11,500 per solid angle. The timing of the various lasers with reference to the time sequence of the AGS is also discussed.

On looking at the commercially available low-intensity light imaging systems, we have found that the Hamamatsu V2025U well suits this project. Appendix IV gives the specifications for this imaging system. Using the phosphorous screen-type output, the device is able to image light with an intensity range from 10^1 to 10^8 photons per second per mm^2 using micro-channel plates for intensifying extremely weak images. The spectral range of the device is 280 to 650 nanometers with a peak response at 420 nm or 7.14×10^{14} Hz. Another possible imaging system is one implementing a charge-coupled device (CCD) preceded by several micro-channel plates and a photo-cathode. This set-up would facilitate the electronic storage of the image in a computer. Information concerning the CCD's manufactured by Tektronix is also given in Appendix IV.

If the YAG laser is used, the detector can be placed at any scattering angle between 97° and 118°. This will allow for the imaging of both high and low intensity proton beams, 0.2 to 30 GeV. If the CO2 is used, the angular range for 30 GeV protons is 152° to 161°. If the detector is positioned at a larger angle, a larger energy range will be accessible. At a scattering angle of 160°, the CO2 will allow for imaging of protons with energies from 1.8 to 30 GeV. It should be noted, however, that the number of scattered photons per solid angle is inversely proportional to γ^2 where $\gamma = 1/\sqrt{1 - v^2/c^2}$. If the energy of the protons is 30 GeV, $\gamma = 30$ and the number of scattered photons is in the thousands. If the energy is 0.2 GeV, $\gamma = 1.2$ and the number of photons is in the tens. The chosen detector should have a sufficiently powerful image intensifying system to "see" the low energy proton beam.

The two graphs following this summary show the type of data that can be expected from the proposed imaging system. In the computer simulation, the minimum number of photons was used (1140, corresponding to a YAG laser and a detector with a 20% quantum efficiency.) The scattered photons are assumed to be normally distributed in accordance with a Gaussian distribution. The standard deviations are based on experimental data from the current monitoring system. The schematic diagram following the graphs presents a possible physical arrangement for the apparatus in the AGS. A scattering angle of $\theta = 110°$ is used, corresponding to a peak response in the V2025U. The laser used is the YAG, placed far enough away from the interaction point so that the collision is approximately head-on. The only physical constraints inherent in this system are that the laser beam must approach the proton beam as close to head-on as possible and that a large converging lens be used near the interaction point to maximize the collection of scattered photons. Though the ten-foot straight section shown in the diagram is suitable, the system could fit just as well elsewhere.

Considerable additional study is still needed since this sketch does not place the detector along the beam line as is assumed in the calculations; therefore, the photons detected here will be far fewer than shown in Figures 1 and 2.

An in-depth study of both the physics and engineering aspects of a laser-based system for beam diagnostics in the AGS suggests that this proposal is both theoretically and practically well-founded. Such a system would allow for accurate, non-destructive beam imaging over the full energy spectrum of the AGS.

I would like to thank Dr. E. Bleser for proposing this problem to me and for supporting me throughout my research.

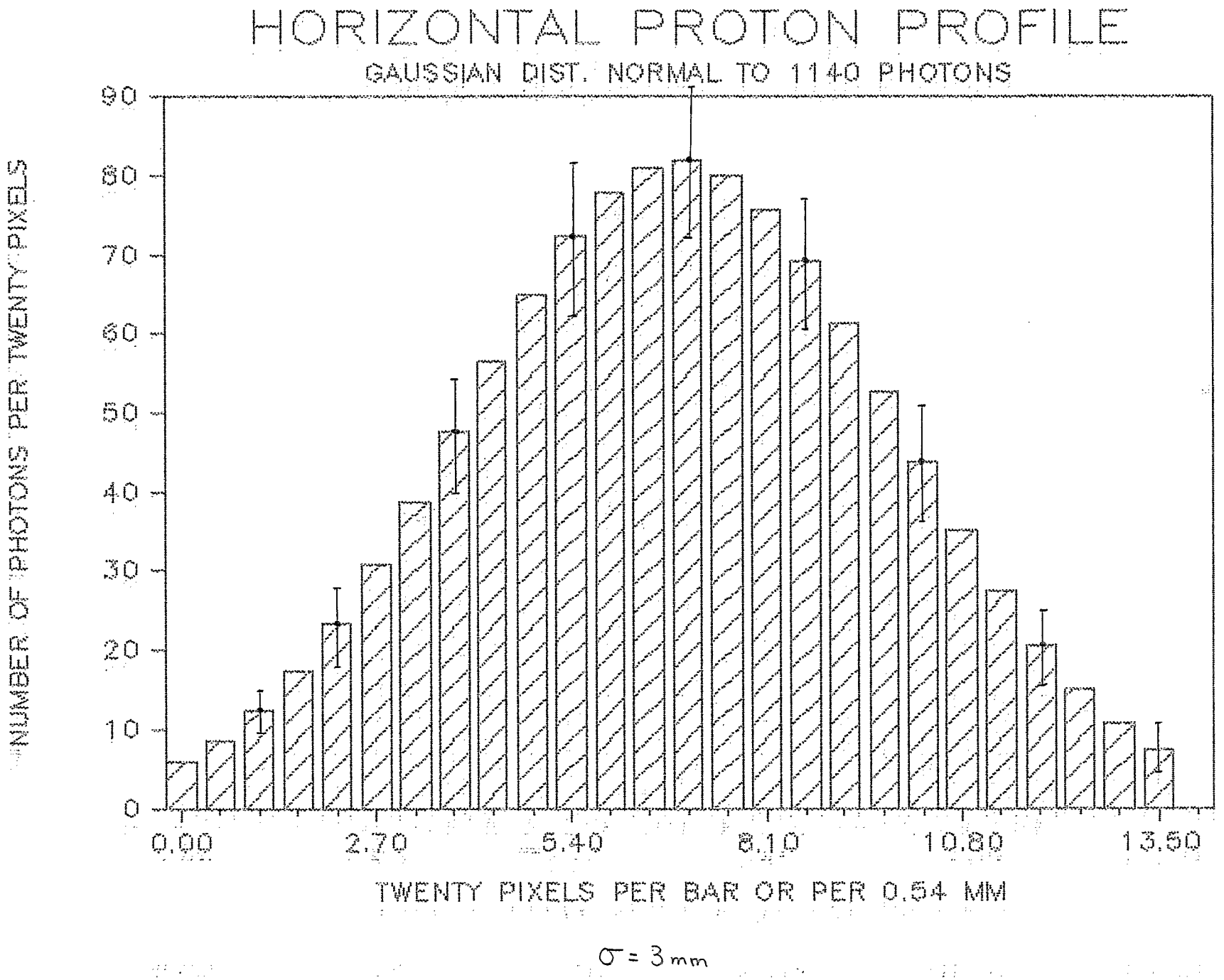
HORIZONTAL PROTON PROFILE
GAUSSIAN DIST. NORMAL TO 1140 PHOTONS
NUMBER OF PHOTONS PER TWENTY PIXELS
90
80
70
60
50
40
30
20
10
0
0.00
2.70
5.40
8.10
10.80
13.50
TWENTY PIXELS PER BAR OR PER 0.54 MM
σ = 3 mm

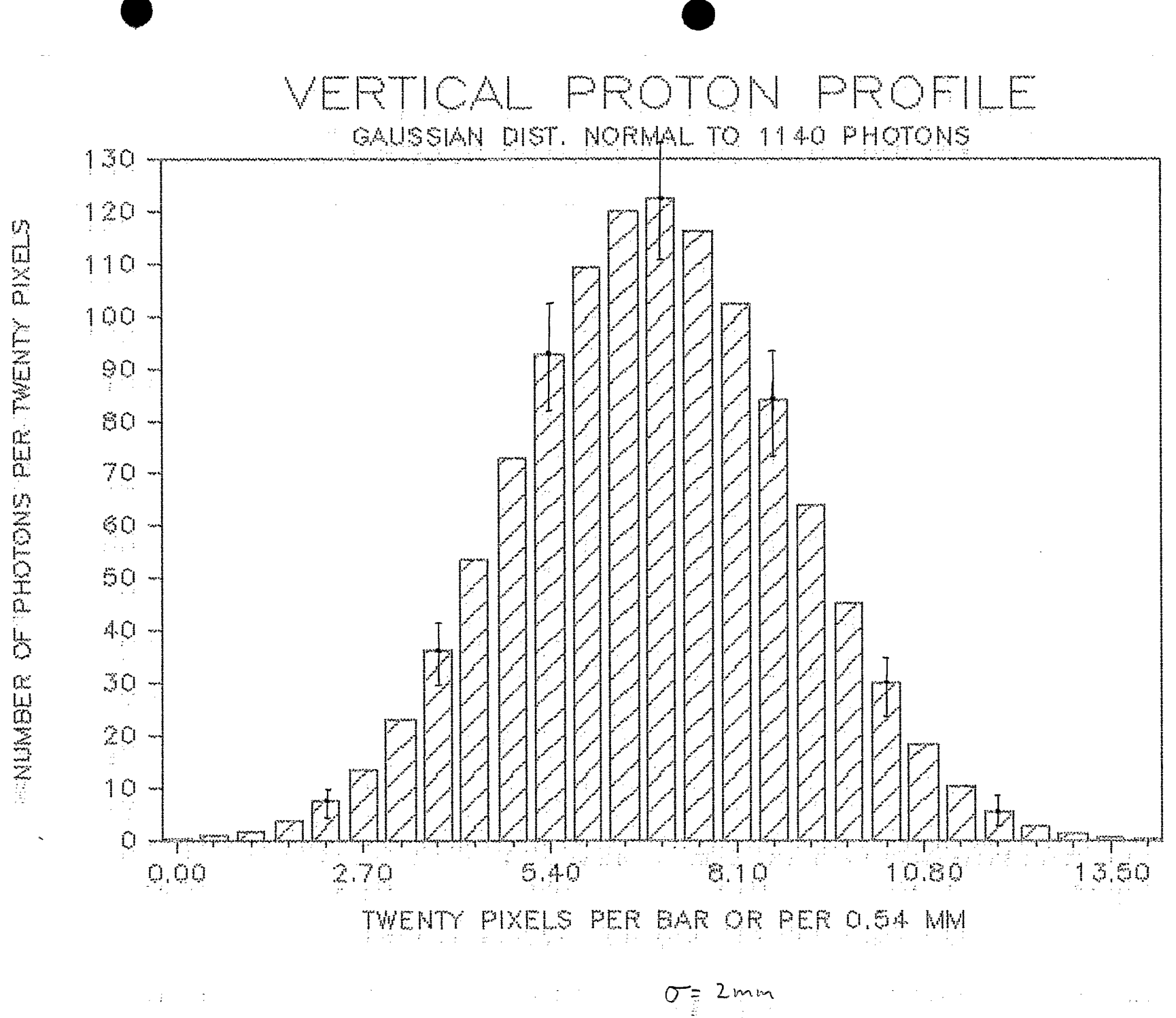
VERTICAL PROTON PROFILE
GAUSSIAN DIST. NORMAL TO 1140 PHOTONS
NUMBER OF PHOTONS PER TWENTY PIXELS
130
120
110
100
90
80
70
60
50
40
30
20
10
0
0.00
2.70
5.40
8.10
10.80
13.50
TWENTY PIXELS PER BAR OR PER 0.54 MM

$\sigma = 2mm$

(SPECIFICALLY : [redacted])

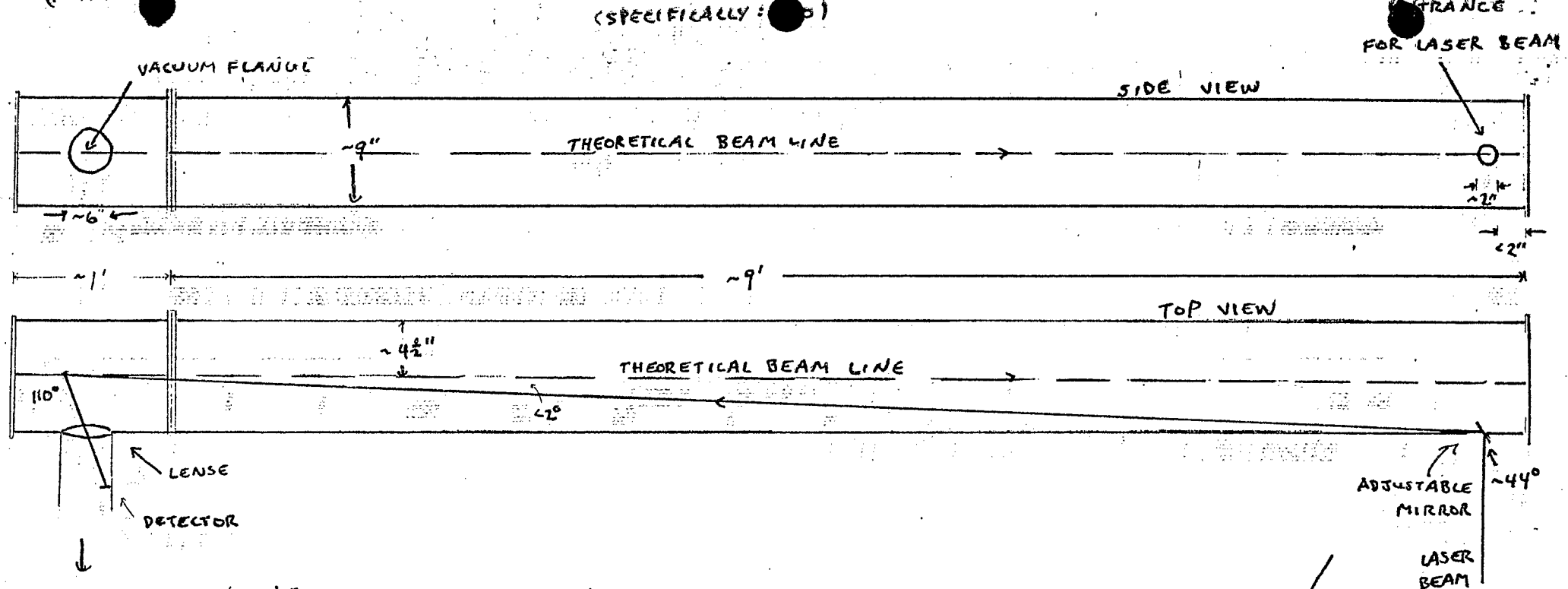

(1" = ¼")

THESE NUMBERS ARE ESTIMATES

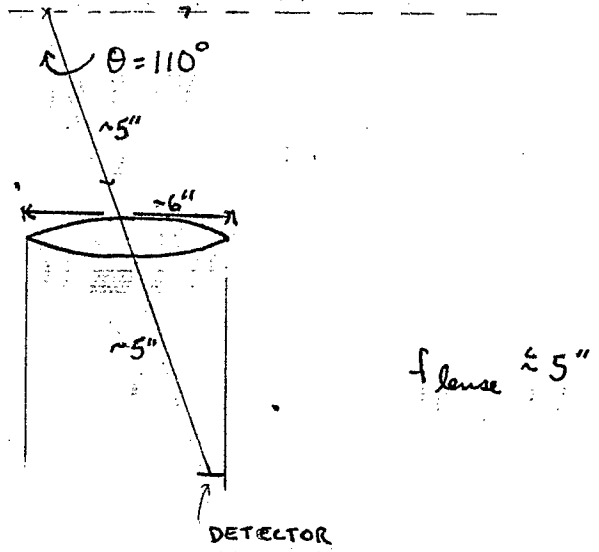

$f_{lense} \approx 5"$

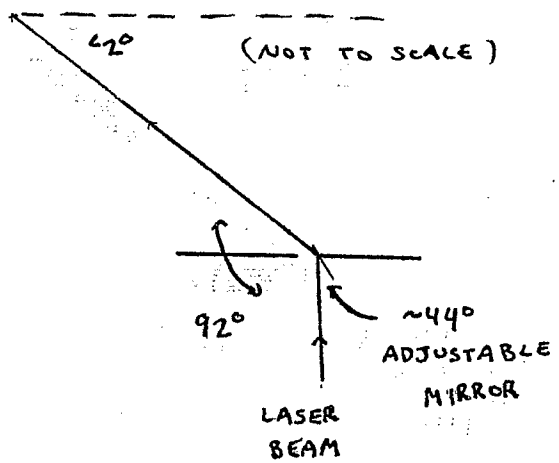

$$d\Omega \approx \frac{A}{\ell^2} = \frac{\pi(\frac{6"}{2})^2}{(5")^2}$$

$$d\Omega \approx 1$$

Appendix I: The Collision Cross-Section

The proposal to implement a laser-based detection system in the AGS must first be studied in the simplified model of a one-on-one photon-proton collision. The Klein-Nishina Equation gives the differential cross-section, $d\sigma$, for the collision of a photon of incident frequency, ν_o, with a particle at rest, usually an electron, but in our case, a proton. The equation is given by Evans in The Atomic Nucleus, page 680, as

$$d\sigma = \frac{r_o^2}{2} d\Omega \left(\frac{\nu_f}{\nu_o}\right)^2 \left(\frac{\nu_f}{\nu_o} + \frac{\nu_o}{\nu_f} - 2 \sin^2 \theta \cos^2 \eta\right) \left[\frac{cm^2}{proton}\right] \qquad (1)$$

where $r_o = e^2/m_o c^2$ in CGS units, ν_f is the frequency of the scattered radiation, $d\Omega$ is the solid angle given by $\sin \theta \, d\theta \, d\phi$, θ is the scattering angle and η specifies the polarization of the incident photon. Given the relation between the incident and scattered frequencies, Eq. 1 can be used to calculate the probability of a specific collision occurring between a photon of frequency ν_o and a proton when the photon passes through a material whose surface density is 1 proton/cm^2. The collision is such that the scattered photon has frequency ν_f and is scattered through an angle θ within the solid angle $d\Omega$. A sum has been done over all polarizations of the scattered photon since the polarization of the scattered photon is experimentally unimportant. $d\sigma$ is called the collision cross-section.

Using an equation derived from a study of the Compton Effect, we find that

$$\frac{\nu_f}{\nu_o} = \frac{1}{1 + \alpha (1 - \cos \theta)} \qquad (2)$$

where $\alpha = h\nu_o/m_o c^2$ and θ is again the scattering angle. Eq. 1 becomes

$$\left(\frac{d\sigma'}{d\Omega'}\right) = \frac{r_o^2}{2} \left(\frac{1}{1 + \alpha' (1 - \cos \theta')}\right)^2 \left[\frac{1}{1 + \alpha' (1 - \cos \theta')} + \right.$$

$$\left. (1 + \alpha' (1 - \cos \theta')) - 2 \sin^2 \theta' \cos^2 \eta'\right] \qquad (3)$$

This describes the collision between a photon and a proton, providing that the proton is initially at rest. However, in the AGS, the protons assume speeds of up to 0.99944c. Eq. 3 is only correct in the rest frame of the proton. This will be the primed reference frame, denoted '. If the incident photon has a frequency of α (frequency will often be represented by the unitless $\alpha = h\nu_o/m_oc^2$) in the lab frame, the effect of the proton's motion will cause a Doppler shift in the photon's frequency as seen by the proton. The proton sees a photon approaching with frequency

$$\alpha' = \alpha\gamma\ (1 - \beta \cos \phi) \tag{4}$$

where $\gamma = \dfrac{1}{\sqrt{1 - v^2/c^2}}$ (= 30 in the AGS), $\beta = v/c$ (= 0.99944 in the AGS) and ϕ is the angle between the direction of motion of the proton and the photon measured in the lab frame. For example, for a head-on collision between the proton and the photon, $\phi = 180°$. Also, the scattering angle θ seen in the lab frame is not the θ' appearing in Eq. 3. They are related by

$$\theta' = \tan^{-1}\left[\frac{\sin\theta}{\gamma\ (\cos\theta - \beta)}\right] \tag{5}$$

The solid angle, $d\Omega'$, must also be transformed to the lab frame. To do this, we must determine the relation between $d\Omega'$ and $d\Omega$. The solid angle is defined as

$$d\Omega' = \frac{dA'}{R'^2} = \sin\theta'\ d\theta'\ d\phi'$$

where $dA' = R'^2 \sin\theta'\ d\theta'\ d\phi$, a surface element on a sphere of radius R'. For our purposes

$$d\Omega' = \frac{dA'}{R'^2}$$

where dA' is the area of the detector and R' is the distance from the point of interaction to the detector as measured by the proton.

If the detector is placed along the line of motion of the proton (this will turn out to be the position of the most experimental interest), then the proton sees the distance to the detector contracted:

$$R' = \frac{R_o}{\gamma} \tag{6}$$

where R_o is the rest length from the collision point to detector, measured in the lab frame. $dA = dA'$ because the motion of the proton is perpendicular to the area element. Therefore,

$$d\Omega' = \frac{dA'}{R'^2} = \gamma^2 \frac{dA}{R_o^2} = \gamma^2 \, d\Omega$$

$$d\Omega' = 900 \, d\Omega$$

This relation holds for the special cases of backscattered radiation ($\theta = 180°$) if the incident radiation is either parallel of anti-parallel to the motion of the proton ($\phi = 0°$ or $180°$). The calculation is also correct for an approach perpendicular to the motion of the proton ($\phi = 90°$) if the detector is located to detect radiation scattered at $\theta = 90°$.

Using the transformation of the solid angle and Eqs. 4 and 5 completes the transformation of the Klein-Nishina Equation to one which is applicable to the situation at hand, a photon striking a proton moving at relativistic speeds:

$$\frac{d\sigma}{d\Omega} = 900 \frac{r_o^2}{2} \left[\frac{1}{1 + \alpha\gamma \, (1 - \beta \cos \phi)\left(1 - \cos \left(\tan^{-1} \left[\frac{\sin \theta}{\gamma(\cos \theta - \beta)}\right]\right)\right)} \right]^2$$

$$\left[1 + \alpha\gamma \, (1 - \beta \cos \phi)\left(1 - \cos \left(\tan^{-1} \left[\frac{\sin \theta}{\gamma \, (\cos \theta - \beta}\right]\right)\right) + \right.$$

$$\frac{1}{1 + \alpha\gamma \, (1 - \beta \cos\phi) \left(1 - \cos \left(\tan^{-1} \left[\frac{\sin \theta}{\gamma \, (\cos \theta - \beta)}\right]\right)\right)} -$$

$$\left. 2 \sin^2 \left(\tan^{-1} \left[\frac{\sin \theta}{\gamma \, (\cos \theta - \beta)}\right]\right) \cos^2 \eta' \right]$$

The problem now becomes one of maximizing the collision cross-section. The factor of r_o^2 on the right-hand side of Eq. 3 is on the order of 10^{-32}. In order that the collision have some reasonable liklihood of occurring the other terms on the right must be maximized. Immediately, the polarizaton of the incident photon should be set so that $\eta' = \pi/2$. To be precise, η' is the angle between the plane of polarization of the incident photon and the scattering plane as measured in the proton's rest frame.

To determine η in the lab frame, we set up our axes so that the motion of the proton frame is along the z-axis of the lab's coordinate system. For our convenience, let the origins of the coordinate systems be coincident at the instant of the collision. Afterwards, what do they see?

If the photon was incident along the z-axis, it was also incident along the z'-axis. After the collision, the photon is scattered by some angle θ in the lab frame, measured as θ' in the proton frame. Assume that the polarization of the photon is along the x-axis, then it is also along the x'-axis because the relative motion of the reference frames is in the zz'-direction.

If $\eta' = \pi/2$, then the photon is scattered in the y'z'-plane. The diagrams below illustrate that the motion of the proton frame with respect to the lab frame does not result in raising the scattered photon from the yz-plane. Therefore, if $\eta' = \pi/2$, then η also equals $\pi/2$.

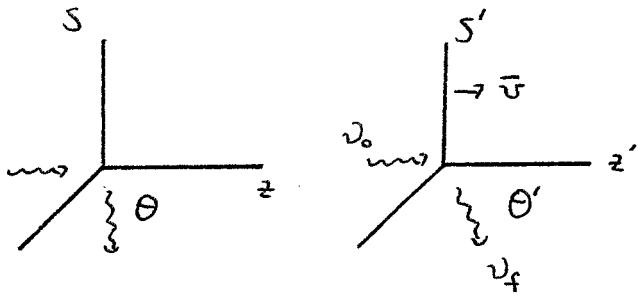

$$\eta' = \frac{\pi}{2}$$

In the case of a photon approaching perpendicular to the motion of the proton, we set up our axes in a slightly different manner. Let the proton frame move along the negative xx'-axes and let the photon approach along the y-axis. Because of the motion of the proton's reference frame with respect to the lab frame, the proton will see a photon approaching, not along the y'-axis, but at some angle to it in the x'y'-plane. We take the polarization of the photon to be along the zz'-axes. If η' is to be $\pi/2$, then we are looking at photons scattered in the x'y'-plane. Because of the fortuitous choice of axes, η will also be equal to $\pi/2$ if we look for scattering in the xy-plane. Therefore, regardless of the angle of incidence (ϕ = 0°, 90° or 180d), if $\eta' = \pi/2$, $\eta = \pi/2$.

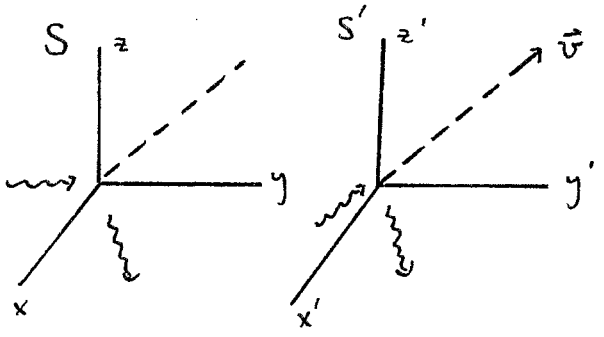

Using this value for η', the last term in Eq. 3 vanishes and we have

$$\frac{d\sigma}{d\Omega} = 900\,\frac{r_o^2}{2}\left(\frac{1}{1+\alpha'(1-\cos\theta')}\right)^2\left[\frac{1}{1+\alpha'(1-\cos\theta')} + 1+\alpha'(1-\cos\theta')\right] \qquad (7)$$

If we let $\psi = 1 + \alpha'(1 - \cos\theta')$, Eq. 7 looks like

$$\frac{d\sigma}{d\Omega} = 900\,\frac{r_o^2}{2}\,\frac{1}{\psi^2}\left(\psi + \frac{1}{\psi}\right).$$

In order to maximize $d\sigma/d\Omega$, ψ should be minimized. In other words, let $\psi = 1 + \alpha'(1 - \cos\theta') \to 1$. This turns out to be relatively easy. Remember, $\alpha' = \alpha\gamma(1 - \beta\cos\phi)$, so we simply let $\alpha \to 0$. As $\alpha \to 0$, $\alpha' \to 0$ and $\psi \to 1$ for all values of the scattering angle and along the axis of the proton beam $d\sigma/d\Omega \to 900\, r_o^2$, which is the maximum cross-section attainable for this particular collision. This is a very good approximation since α is very tiny. The photon energy is a few electron volts while the proton mass is a billion electron volts. Thus, α is a few parts in a billion. We are working with the proton analogue of Thompson scattering, which in the rest frame of the proton is essentially isotropic in the scattering plane. Therefore, the maximum cross-section for a photon-proton collision is $900\, r_o^2 = 2.1 \times 10^{-29}$ cm^2. However, this was calculated for a material with a proton surface density of 1 proton/cm^2. In the AGS, the proton surface density is significantly higher.

At maximum capacity, the AGS holds approximately 1.5×10^{13} protons in 12 bunches of 1.25×10^{12} protons/bunch. For our purposes, we will approximate a proton pulse with a cylinder of rectangular cross-section. The length of the cylinder can be determined using the time it takes the pulse to pass a detector, approximately 30 nanoseconds, and its speed, $v = 0.99944c$. The length, given by $L = v \times t$, is approximately 900 cm. The cross-sectional area is about 0.06 cm^2, assuming the bunch has a width of 0.3 cm and a height of 0.2 cm. Therefore, the density of protons in a pulse is

$$\rho = 2.3 \times 10^{10} \text{ protons/cm}^3.$$

The proton surface density for either a parallel or anti-parallel approach is

$$\lambda_{\parallel} = (900 \text{ cm})\,\rho = 2.1 \times 10^{13} \frac{\text{protons}}{\text{cm}^2}$$

If the approach is perpendicular to the proton beam, then the surface density is

$$\lambda_{\perp} = (0.03 \text{ cm})\,\rho = 6.9 \times 10^{9} \frac{\text{protons}}{\text{cm}^2}$$

These calculations are only approximations. They do not take into account the irregular shape of the pulse nor the non-uniform density of protons in the pulse. However, they should suffice for our purposes.

These densities represent the multiplicative increase in the target size above the 1 proton/cm^2 for which the previous cross-sections were calculated. Therefore, to determine the total collision cross-sections in the AGS, the previously determined cross-sections should be multiplied by the value of the surface density for that particular collision. If the approach is parallel or anti-parallel to the proton beam,

$$\left(\frac{d\sigma}{d\Omega}\right)_{TOT,\parallel} = \lambda_{\parallel}\ 900\ r_o^2 = 4.3 \times 10^{-16}\ cm^2.$$

If the incident photon approaches perpendicular to the proton's path, then

$$\left(\frac{d\sigma}{d\Omega}\right)_{TOT,\perp} = \lambda_{\perp}\ 900\ r_o^2 = 1.4 \times 10^{-19}\ cm^2.$$

These numbers represent rough upper limits on the collision cross-section for photon-proton collisions in the AGS.

Appendix II: The Frequency Shift

Another issue of experimental importance is the frequency shift of the scattered radiation. Ideally, the backscattered radiation ($\theta = 180°$) would suffer a large frequency shift which would make it experimentally easier to differentiate between the incident and the scattered radiation. Eq. 2 gives the relation between the frequencies of the incident and scattered photons in the rest frame of the proton:

$$\nu'_f = \nu'_o \left[\frac{1}{1 + \alpha' (1 - \cos\theta')}\right] \tag{2}$$

We can transform Eq. 2 to the lab frame using the transformation equations:

$$\nu'_o = \nu_o \gamma (1 - \beta \cos\phi)$$

$$\alpha' = \alpha\gamma (1 - \beta \cos\phi)$$

$$\nu'_f = \nu_f \gamma (1 - \beta \cos\phi_f)$$

$$\theta' = \tan^{-1}\left[\frac{\sin\theta}{\gamma(\cos\theta - \beta)}\right]$$

introducing the angle ϕ_f between the direction of motion of the scattered photon and the proton. Remember that ϕ is the angle between the incident photon and the proton. Eq. 2 becomes

$$\nu_f \gamma (1 - \beta \cos\phi_f) = \nu_o \gamma (1 - \beta \cos\phi)$$

$$\left[\frac{1}{1 + \alpha\gamma (1 - \beta\cos\phi)\left(1 - \cos\left(\tan^{-1}\left[\frac{\sin\theta}{\gamma(\cos\theta - \beta)}\right]\right)\right)}\right] \tag{8}$$

The behavior of Eq. 8 is not exactly intuitively obvious. If we let the term in brackets on the right be represented by ψ, Eq. 8 becomes

$$\nu_f \gamma (1 - \beta \cos\phi_f) = \nu_o \gamma (1 - \beta \cos\phi)\psi \tag{9}$$

Since α is very, very small, $\Psi \to 1$ and Eq. 9 becomes:

$$\frac{\nu_f}{\nu_o} = \frac{1 - \beta \cos \phi}{1 - \beta \cos \phi_f}.$$

If $\phi = 0°$, an approach from behind, ϕ_f is the same angle as θ, the scattering angle (see Fig. 1 below). In this case,

$$\left(\frac{\nu_f}{\nu_o}\right)_{\phi=0°} = \frac{1 - \beta}{1 - \beta \cos \phi_f} \xrightarrow{\theta \to 180°} 2.8 \times 10^{-4}$$

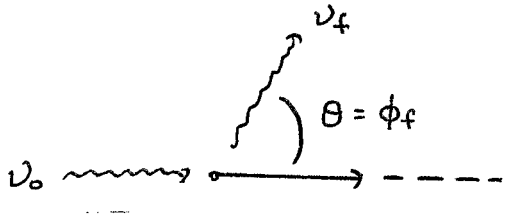

Fig. 1

If ν_o were, for example, 2.8×10^{14} Hz (YAG laser), then the frequency of the back scattered radiation would be 7.8×10^{10} Hz. This corresponds to a frequency shift from the infra-red region of the spectrum to the microwave. See Graph 1.

If $\phi = 90°$,

$$\left(\frac{\nu_f}{\nu_o}\right)_{\phi=90°} = \frac{1}{1 - \beta \cos \phi_f} \quad \text{where} \quad \begin{array}{l} \phi_f = 90° - \theta \quad 0 \leq \theta \leq 90° \\ \phi_f = \theta - 90° \quad 90° \leq \theta \leq 180° \end{array}$$

See Fig. 2a and 2b. In this case, the largest frequency shift is seen for a scattering angle of 90°.

$$\left(\frac{\nu_f}{\nu_o}\right)_{\phi=90°} \xrightarrow[\theta \to 90°]{} 1800.$$

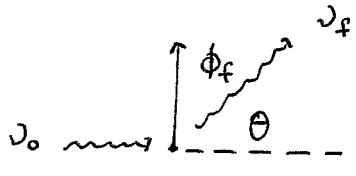

Fig. 2a.

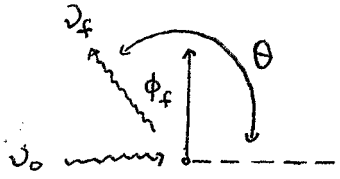

Fig. 2b.

If $\nu_o = 2.8 \times 10^{14}$ Hz, $\nu_f = 5.0 \times 10^{17}$ Hz. This represents a shift from the infrared region to the ultra-violet. For this particular angle of incidence, perpendicular to the proton's motion, the frequency shift for backscattered radiation is negligible. As $\theta \to 180°$, $\nu_f/\nu_o \to 1$. See Graph 2.

Lastly, for a head-on collision, $\phi = 180°$, $\phi_f = 180° - \theta$. See Fig. 3 below. Eq. 10 becomes

$$\left(\frac{\nu_f}{\nu_o}\right)_{\phi=180°} = \frac{1 + \beta}{1 - \beta \cos (180° - \theta)}$$

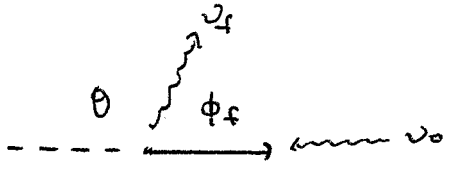

Fig. 3.

As $\theta \to 180°$:

$$\left(\frac{\nu_f}{\nu_o}\right)_{\phi=180°} \xrightarrow[\theta \to 180°]{} 3600$$

For $\nu_o = 2.8 \times 10^{14}$ Hz, $\nu_f = 1.0 \times 10^{18}$ Hz, a shift from the infrared to the x-ray. See Graph 3.

Collectively, the graphs illustrate that there are several experimental alternatives which would result in a large frequency shift of the scattered radiation.

GRAPH 1

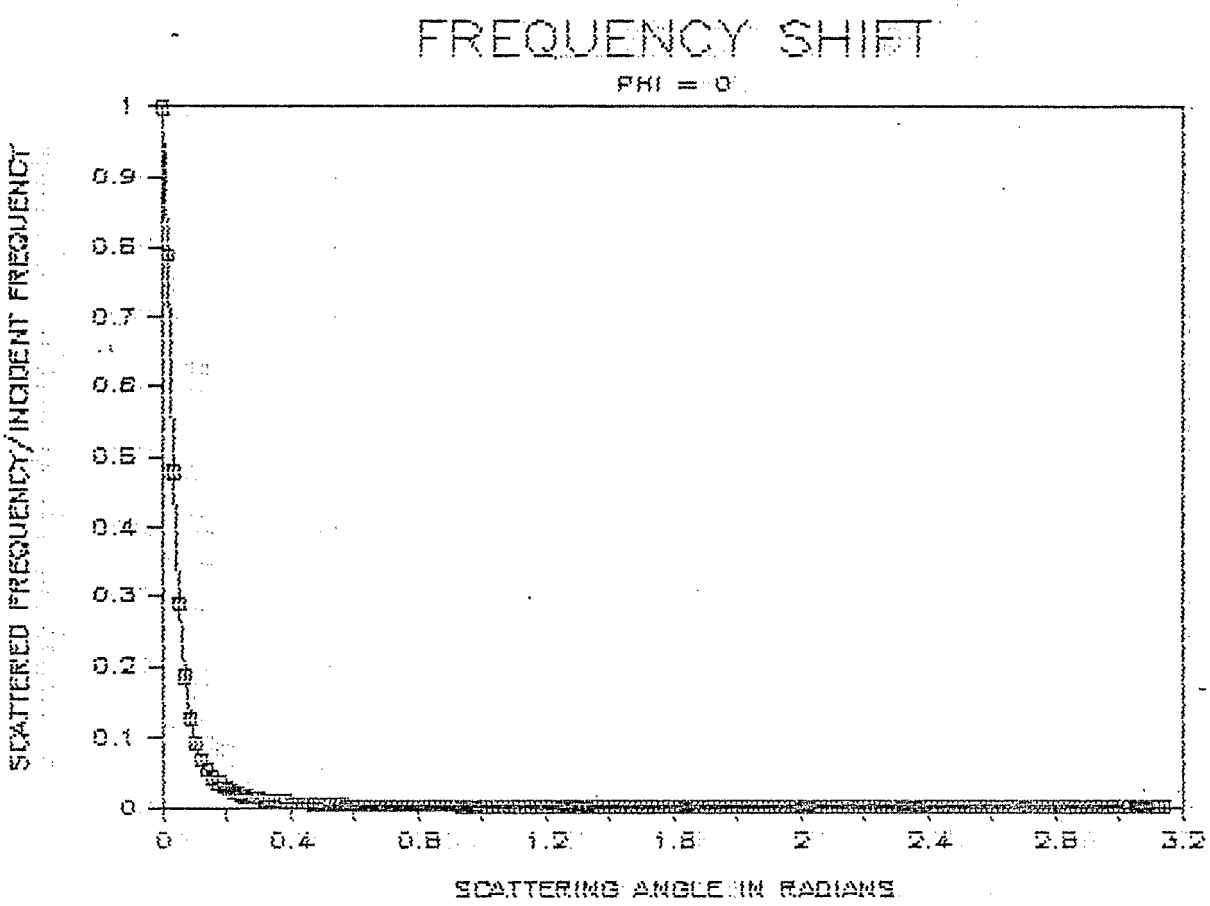
FREQUENCY SHIFT
PHI = 0
SCATTERED FREQUENCY/INCIDENT FREQUENCY
1
0.9
0.8
0.7
0.6
0.5
0.4
0.3
0.2
0.1
0
0
0.4
0.8
1.2
1.8
2
2.4
2.8
3.2
SCATTERING ANGLE IN RADIANS

GRAPH 2

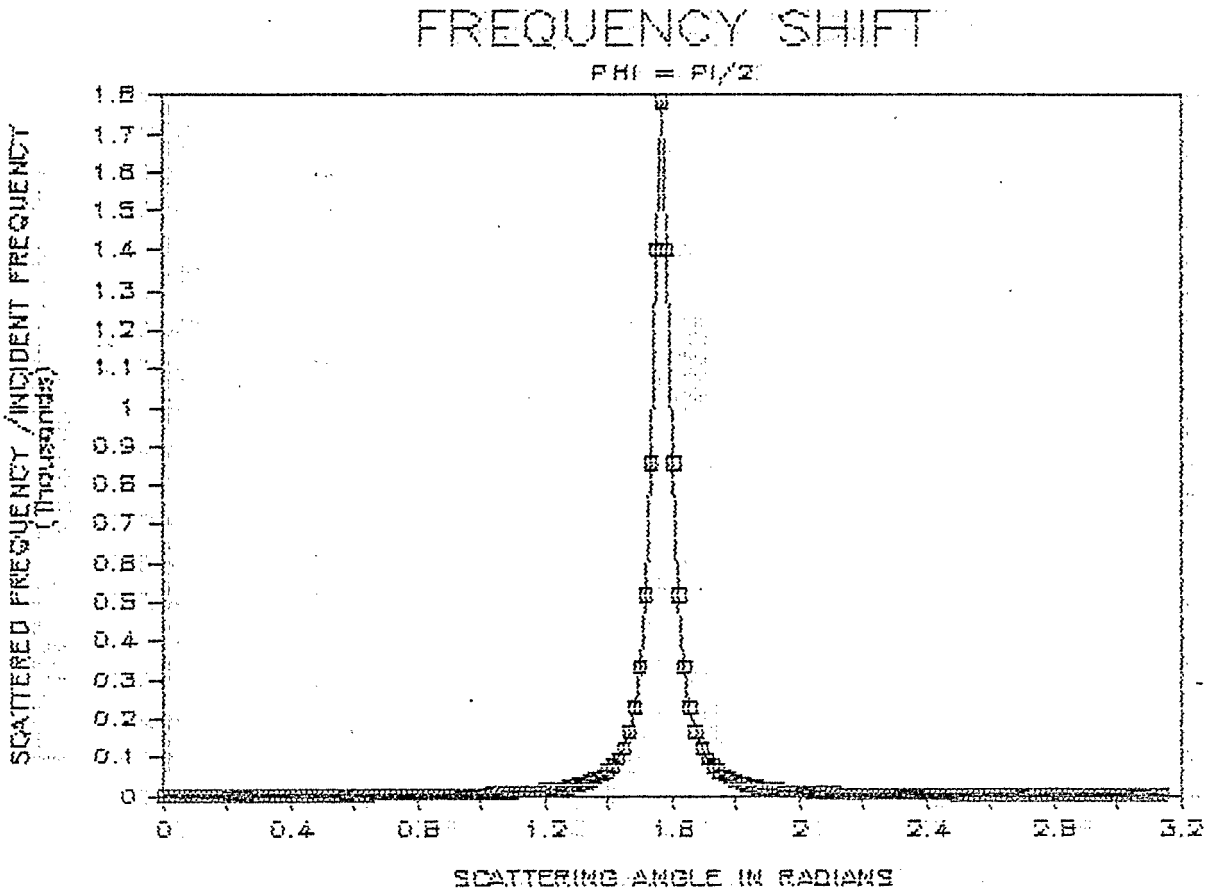
FREQUENCY SHIFT
PHI = PI/2
SCATTERED FREQUENCY /INCIDENT FREQUENCY
(Thousands)
1.8
1.7
1.6
1.5
1.4
1.3
1.2
1.1
1
0.9
0.8
0.7
0.6
0.5
0.4
0.3
0.2
0.1
0
0
0.4
0.8
1.2
1.6
2
2.4
2.8
3.2
SCATTERING ANGLE IN RADIANS

GRAPH 3

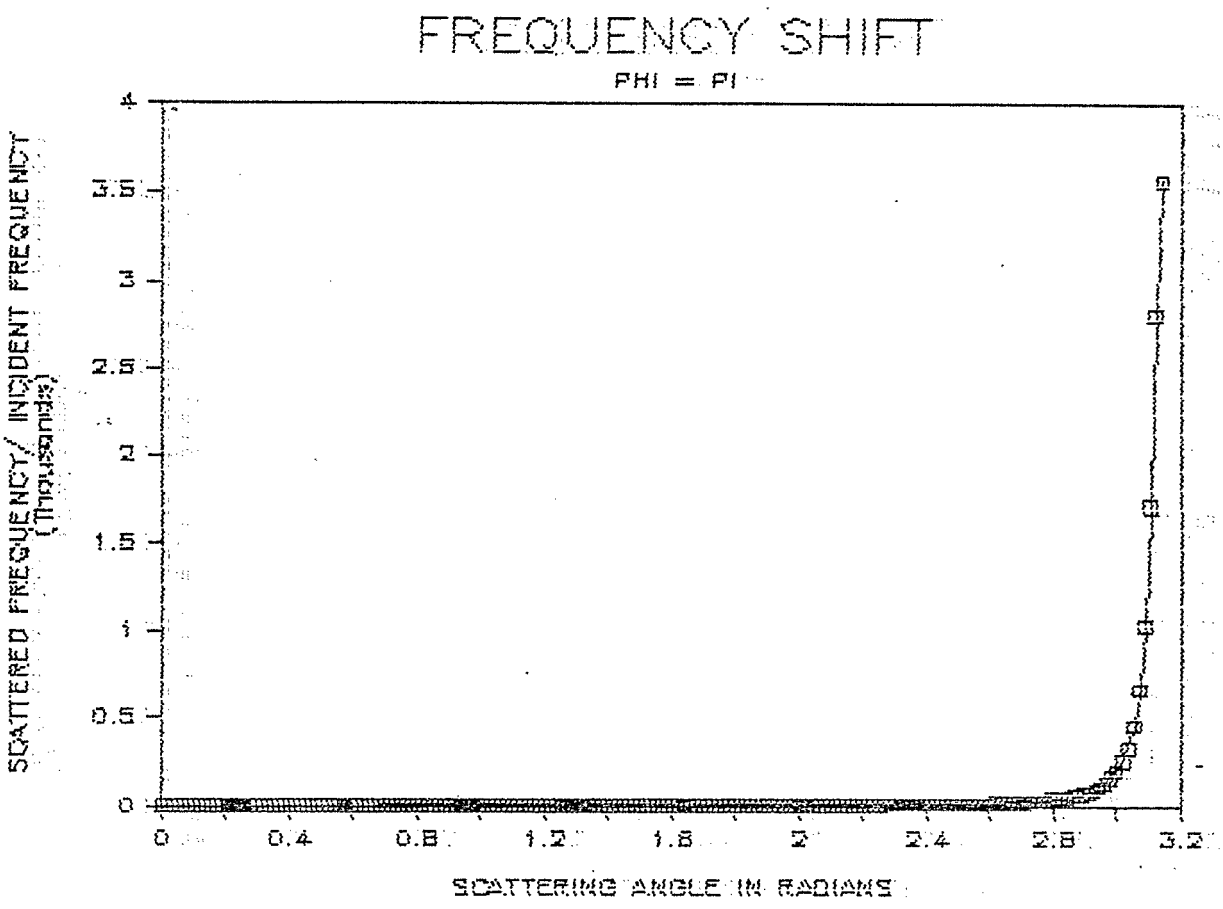
FREQUENCY SHIFT
PHI = PI
SCATTERED FREQUENCY/ INCIDENT FREQUENCY (Thousands)
0
0.5
1
1.5
2
2.5
3
3.5
4
0
0.4
0.8
1.2
1.6
2
2.4
2.8
3.2
SCATTERING ANGLE IN RADIANS

Appendix III: Lasers

Now that we have calculated the collision cross-sections, we can determine how many photons will actually reach a detector. If ν_0 is the incident frequency of the laser pulse and E_0 is the energy per pulse, then

$$n_o = \frac{E_o}{h\nu_o}$$

is the number of incident photons per pulse. If S is the cross-sectional area of the proton beam (assumed to be approximately 0.06 cm^2 for a parallel or anti-parallel approach and 180 cm^2 for a perpendicular approach, see figure) and if we use lenses to match the cross-section of the laser pulse with that of the proton pulse, then n_0/S is the number of incident photons per cm^2 in a pulse. Therefore,

$$\frac{dN}{d\Omega} = \frac{n_o}{S} \frac{d\sigma}{d\Omega}$$

is the total number of photons scattered through the differential solid angle, $d\Omega$, from a single laser pulse - proton pulse interaction.

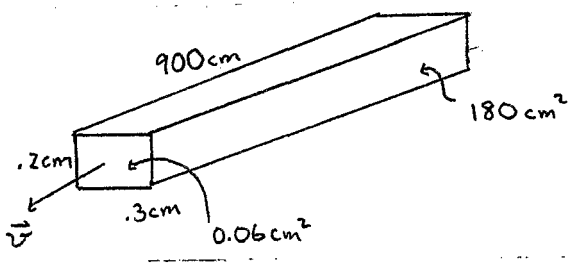

The following page gives some of the relevant information for a few of the available lasers. The time, t, displayed is the length of the pulse. The power, P_o, is the power per pulse or E_0/t. The last two columns give $dN/d\Omega$ for parallel or anti- parallel approaches ($N/d\Omega$ II) and for a perpendicular approach ($N/d\Omega$ PER). In our calculations, we use the previously determined values for $d\sigma/d\Omega$:

$$\left(\frac{d\sigma}{d\Omega}\right)_{tot,11} = 4.3 \times 10^{-16} cm^2$$

$$\left(\frac{d\sigma}{d\Omega}\right)_{tot,\perp} = 1.4 \times 10^{-19} cm^2$$

DATA ON SPECIFIC LASERS

laser	λ_o [nm] wavelgnth	υ_o [Hz] freqcy	d [cm] beam dia	t [ns] time	E_o [J] energy	no photons	P_o [W] power
CO2	10600	2.8E+13	0.5	50	0.03	1.6E+18	600000
DF1	3600	8.3E+13	0.2	50	0.002	3.6E+16	40000
HF1	2600	1.2E+14	0.2	50	0.002	2.6E+16	40000
YAG	1064	2.8E+14	0.075	50	0.15	8.0E+17	3000000
ArF1	193	1.6E+15	2	10	0.03	2.9E+16	3000000
KrCl	249	1.2E+15	2	20	0.04	5.0E+16	2000000
XeCl	308	9.7E+14	2	20	0.225	3.5E+17	11250000
XeF1	351	8.5E+14	2	20	0.006	1.1E+16	300000

laser	η/cm^2 II	η/cm^2 PER	N/dΩ II	N/dΩ PER
CO2	2.7E+19	8.9E+15	11464.93	0.001244
DF1	6.0E+17	2.0E+14	259.3834	0.000028
HF1	4.4E+17	1.5E+14	187.4769	0.000020
YAG	1.3E+19	4.3E+15	5754.100	0.000624
ArF1	4.9E+17	1.6E+14	208.7483	0.000022
KrCl	8.4E+17	2.8E+14	359.0904	0.000038
XeCl	5.8E+18	1.9E+15	2498.490	0.000271
XeF1	1.8E+17	5.9E+13	75.92816	0.000008

The CO_2 laser comes out ahead with 11,500 photons scattered per differential solid angle. The YAG is the runner-up with 5800 photons. These numbers represent the maximum number of photons that can be expected to scatter through the differential scattering angle $d\Omega$.

In deciding which laser should ultimately be used for the project, other technical details must addressed. To begin with, the laser pulse should physically match the proton pulse as closely as possible. For instance, as mentioned previously, lenses should be used to converge or diverge the laser beam so that its cross-section is about that of the proton pulse. Also, the length of the laser pulse should match the proton pulse, 30 - 60 nanoseconds. Both the CO_2 and the YAG have 50 nanosecond pulses which fit nicely in the acceptable range.

Ideally, the time sequence of the laser would match that of the AGS. Unfortunately, this is impossible. The period of a pulse in the AGS is 2.7 microseconds, much faster than most lasers. This number is calculated from the circumference of the AGS ($2 \cdot \pi \cdot 13{,}000$ cm) and the speed of the protons (approximately c). Q-switched lasers have frequencies in the 0.1 - 300 Hz range, a maximum of one pulse every 3.3 milliseconds.

Though the laser cannot match the period of the proton pulse, it can be set to match a large integral number of proton revolutions. To estimate the minimum number of revolutions a specific proton pulse must make between laser pulses, we take the period of the laser pulse and divide it by the period of the proton pulse. If the period of the laser is 3.3 msec and that of the proton pulse is 2.7 microsec, then the laser pulse can be made to collide with a specific proton pulse every 1222 revolutions. This large number of revolutions may pose some technological difficulties, depending on the stability of the proton beam. However, using a Q-switched laser, it is theoretically possible to synchronize the laser with an integral number of proton revolutions, which would allow for imaging of a specific proton pulse.

The next consideration is the frequency shift suffered by the laser. In order to image the beam, the frequency of the scattered radiation must fall in the visible range ($3.9 - 7.7 \times 10^{14}$ Hz). This requirement is actually very exclusive, as the data on the following pages illustrates. The frequency of the scattered radiation for several different lasers is displayed. Above each column is first the incident angle ($ze = \phi = 0°$, $ni = \phi = 90°$; $\pi = \phi = 180°$) followed by a slash and then the scattering angle ($\theta = 0°, 10°, \ldots, 180°$). As can

be seen, none of the lasers are scattered into the visible region for an approach from behind (ϕ = ze = 0°). For ϕ = 90°, a perpendicular approach, several possibilities exist. However, the scattering cross-section for this approach is significantly smaller than for a parallel or anti-parallel approach.

For a head-on approach ($\theta = \pi = 180°$), the CO_2 laser scatters light into the visible range at a scattering angle of 150°. For the YAG, the scattering angle must be between 60 and 100 degrees. Which laser is finally adopted for the project depends a great deal on the physical restrictions imposed by the AGS. We should note that both the CO_2 and the YAG have incident frequencies in the infra-red. Scattered radiation in the visible region should allow for relatively easy differentiation between stray incident photons and the scattered photons.

Eleven thousand five hundred scattered photons should like a lot of light. Unfortunately, most detection systems have a quantum efficiency of 20%. Immediately, 11,500 photons/$d\Omega$ becomes 2300 photons. In the case of the YAG laser, we now have 1140 photons. So few photons will require a special detection system.

FREQUENCY OF SCATTERED RADIATION FOR SPECIFIC LASERS ($\phi=0^{\circ}$)

laser	ze/0	ze/10	ze/20	ze/30	ze/40	ze/50	ze/60
CO2	2.8E+13	1.0E+12	2.6E+11	1.2E+11	6.8E+10	4.4E+10	3.2E+10
DF1	8.3E+13	3.0E+12	7.7E+11	3.5E+11	2.0E+11	1.3E+11	9.3E+10
HF1	1.2E+14	4.1E+12	1.1E+12	4.8E+11	2.8E+11	1.8E+11	1.3E+11
YAG	2.8E+14	1.0E+13	2.6E+12	1.2E+12	6.7E+11	4.4E+11	3.2E+11
ArF1	1.6E+15	5.5E+13	1.4E+13	6.5E+12	3.7E+12	2.4E+12	1.7E+12
KrC1	1.2E+15	4.3E+13	1.1E+13	5.0E+12	2.9E+12	1.9E+12	1.3E+12
XeC1	9.7E+14	3.5E+13	9.0E+12	4.1E+12	2.3E+12	1.5E+12	1.1E+12
XeF1	8.5E+14	3.0E+13	7.9E+12	3.6E+12	2.0E+12	1.3E+12	9.6E+11

laser	ze/70	ze/80	ze/90	ze/100	ze/110	ze/120	ze/130
CO2	2.4E+10	1.9E+10	1.6E+10	1.3E+10	1.2E+10	1.1E+10	9.6E+09
DF1	7.1E+10	5.6E+10	4.7E+10	4.0E+10	3.5E+10	3.1E+10	2.8E+10
HF1	9.8E+10	7.8E+10	6.5E+10	5.5E+10	4.8E+10	4.3E+10	3.9E+10
YAG	2.4E+11	1.9E+11	1.6E+11	1.3E+11	1.2E+11	1.1E+11	9.6E+10
ArF1	1.3E+12	1.1E+12	8.7E+11	7.4E+11	6.5E+11	5.8E+11	5.3E+11
KrC1	1.0E+12	8.2E+11	6.7E+11	5.7E+11	5.0E+11	4.5E+11	4.1E+11
XeC1	8.3E+11	6.6E+11	5.5E+11	4.6E+11	4.1E+11	3.6E+11	3.3E+11
XeF1	7.3E+11	5.8E+11	4.8E+11	4.1E+11	3.6E+11	3.2E+11	2.9E+11

laser	ze/140	ze/150	ze/160	ze/170	ze/180
CO2	9.0E+09	8.5E+09	8.2E+09	8.0E+09	7.9E+09
DF1	2.6E+10	2.5E+10	2.4E+10	2.4E+10	2.3E+10
HF1	3.7E+10	3.5E+10	3.3E+10	3.3E+10	3.2E+10
YAG	8.9E+10	8.5E+10	8.1E+10	8.0E+10	7.9E+10
ArF1	4.9E+11	4.7E+11	4.5E+11	4.4E+11	4.4E+11
KrC1	3.8E+11	3.6E+11	3.5E+11	3.4E+11	3.4E+11
XeC1	3.1E+11	2.9E+11	2.8E+11	2.7E+11	2.7E+11
XeF1	2.7E+11	2.6E+11	2.5E+11	2.4E+11	2.4E+11

FREQUENCY OF SCATTERED RADIATION FOR SPECIFIC LASERS (ϕ=90°)

laser	ni/0	ni/10	ni/20	ni/30	ni/40	ni/50	ni/60
CO2	2.8E+13	3.4E+13	4.3E+13	5.7E+13	7.9E+13	1.2E+14	2.1E+14
DF1	8.3E+13	1.0E+14	1.3E+14	1.7E+14	2.3E+14	3.6E+14	6.2E+14
HF1	1.2E+14	1.4E+14	1.8E+14	2.3E+14	3.2E+14	4.9E+14	8.6E+14
YAG	2.8E+14	3.4E+14	4.3E+14	5.6E+14	7.9E+14	1.2E+15	2.1E+15
ArF1	1.6E+15	1.9E+15	2.4E+15	3.1E+15	4.3E+15	6.6E+15	1.2E+16
KrC1	1.2E+15	1.5E+15	1.8E+15	2.4E+15	3.4E+15	5.1E+15	9.0E+15
XeC1	9.7E+14	1.2E+15	1.5E+15	1.9E+15	2.7E+15	4.2E+15	7.2E+15
XeF1	8.5E+14	1.0E+15	1.3E+15	1.7E+15	2.4E+15	3.6E+15	6.4E+15

laser	ni/70	ni/80	ni/90	ni/100	ni/110	ni/120	ni/130
CO2	4.7E+14	1.8E+15	5.1E+16	1.8E+15	4.7E+14	2.1E+14	1.2E+14
DF1	1.4E+15	5.3E+15	1.5E+17	5.3E+15	1.4E+15	6.2E+14	3.6E+14
HF1	1.9E+15	7.3E+15	2.1E+17	7.3E+15	1.9E+15	8.6E+14	4.9E+14
YAG	4.6E+15	1.8E+16	5.0E+17	1.8E+16	4.6E+15	2.1E+15	1.2E+15
ArF1	2.6E+16	9.9E+16	2.8E+18	9.9E+16	2.6E+16	1.2E+16	6.6E+15
KrC1	2.0E+16	7.7E+16	2.2E+18	7.7E+16	2.0E+16	9.0E+15	5.1E+15
XeC1	1.6E+16	6.2E+16	1.7E+18	6.2E+16	1.6E+16	7.2E+15	4.2E+15
XeF1	1.4E+16	5.4E+16	1.5E+18	5.4E+16	1.4E+16	6.4E+15	3.6E+15

laser	ni/140	ni/150	ni/160	ni/170	ni/180
CO2	7.9E+13	5.7E+13	4.3E+13	3.4E+13	2.8E+13
DF1	2.3E+14	1.7E+14	1.3E+14	1.0E+14	8.3E+13
HF1	3.2E+14	2.3E+14	1.8E+14	1.4E+14	1.2E+14
YAG	7.9E+14	5.6E+14	4.3E+14	3.4E+14	2.8E+14
ArF1	4.3E+15	3.1E+15	2.4E+15	1.9E+15	1.6E+15
KrC1	3.4E+15	2.4E+15	1.8E+15	1.5E+15	1.2E+15
XeC1	2.7E+15	1.9E+15	1.5E+15	1.2E+15	9.7E+14
XeF1	2.4E+15	1.7E+15	1.3E+15	1.0E+15	8.5E+14

FREQUENCY OF SCATTERED RADIATION FOR SPECIFIC LASERS (ϕ=180°)

laser	pi/0	pi/10	pi/20	pi/30	pi/40	pi/50	pi/60
CO2	2.8E+13	2.9E+13	2.9E+13	3.0E+13	3.2E+13	3.4E+13	3.8E+13
DF1	8.3E+13	8.4E+13	8.6E+13	8.9E+13	9.4E+13	1.0E+14	1.1E+14
HF1	1.2E+14	1.2E+14	1.2E+14	1.2E+14	1.3E+14	1.4E+14	1.5E+14
YAG	2.8E+14	2.8E+14	2.9E+14	3.0E+14	3.2E+14	3.4E+14	3.8E+14
ArF1	1.6E+15	1.6E+15	1.6E+15	1.7E+15	1.8E+15	1.9E+15	2.1E+15
KrCl	1.2E+15	1.2E+15	1.2E+15	1.3E+15	1.4E+15	1.5E+15	1.6E+15
XeCl	9.7E+14	9.8E+14	1.0E+15	1.0E+15	1.1E+15	1.2E+15	1.3E+15
XeF1	8.5E+14	8.6E+14	8.8E+14	9.2E+14	9.7E+14	1.0E+15	1.1E+15

laser	pi/70	pi/80	pi/90	pi/100	pi/110	pi/120	pi/130
CO2	4.2E+13	4.8E+13	5.7E+13	6.8E+13	8.6E+13	1.1E+14	1.6E+14
DF1	1.2E+14	1.4E+14	1.7E+14	2.0E+14	2.5E+14	3.3E+14	4.7E+14
HF1	1.7E+14	2.0E+14	2.3E+14	2.8E+14	3.5E+14	4.6E+14	6.5E+14
YAG	4.2E+14	4.8E+14	5.6E+14	6.8E+14	8.6E+14	1.1E+15	1.6E+15
ArF1	2.3E+15	2.6E+15	3.1E+15	3.8E+15	4.7E+15	6.2E+15	8.7E+15
KrCl	1.8E+15	2.1E+15	2.4E+15	2.9E+15	3.7E+15	4.8E+15	6.7E+15
XeCl	1.5E+15	1.7E+15	1.9E+15	2.4E+15	3.0E+15	3.9E+15	5.4E+15
XeF1	1.3E+15	1.5E+15	1.7E+15	2.1E+15	2.6E+15	3.4E+15	4.8E+15

laser	pi/140	pi/150	pi/160	pi/170	pi/180
CO2	2.4E+14	4.2E+14	9.3E+14	3.6E+15	1.0E+17
DF1	7.1E+14	1.2E+15	2.7E+15	1.1E+16	3.0E+17
HF1	9.8E+14	1.7E+15	3.8E+15	1.5E+16	4.1E+17
YAG	2.4E+15	4.2E+15	9.3E+15	3.6E+16	1.0E+18
ArF1	1.3E+16	2.3E+16	5.1E+16	2.0E+17	5.5E+18
KrCl	1.0E+16	1.8E+16	4.0E+16	1.5E+17	4.3E+18
XeCl	8.3E+15	1.4E+16	3.2E+16	1.2E+17	3.5E+18
XeF1	7.3E+15	1.3E+16	2.8E+16	1.1E+17	3.1E+18

Appendix IV: Photon Counting Imagers

The following pages are taken from the Hamamatsu 1986 catalogue entitled Special Imaging Tubes. They describe two types of photon counting imaging systems manufactured by Hamamatsu, the system with phosphorous screen output and the system with a position-sensitive device (PSD) output. Both systems use micro-channel plates for image intensifying. The phosphorous screen output is able to image light with a greater range of intensity. It works in two modes: analog and photon counting. The analog mode allows for imaging at higher intensities, as many as 10^8 photons per second per mm^2 without saturating the device. At lower intensities, down to just tens of photons, the device uses the photon counting mode to produce images. The PSD device is only suitable for very low intensities. It has greater intensification capabilities, up to 10^9, implementing three micro-channel plates where the phosphorous screen output only uses two. Also, the PSD allows for a further multiplication of the initial signal by a factor of one hundred. However, if the device receives two signals simultaneously, it rejects the data. For this reason, the device using the PSD device is not suited for this project.

To electronically store the image in a computer, the phosphorous screen can be replaced with a charge-coupled device (CCD). A CCD is a silicon based array which allows for two-dimensional electronic imaging. It is made up of picture elements (pixels) which collect electrons and an output register used to read out the information. The micro-channel plates would allow for sufficient multiplication of the signal so that the CCD could "see" the beam. The read-out process preserves the two-dimensional nature of the picture. Tektronix manufactures CCD's for scientific purposes. Some excerpts from their catalogue follow.

Both Tektronix and Hamamatsu are capable of designing a detection system to suit the needs of this project using a combination of micro-channel plate and charge-coupled device technologies.

HAMAMATSU

Special Imaging Tubes

Photon Counting Imagers, Streak Tubes,
X-Ray Image Intensifiers and Related Products

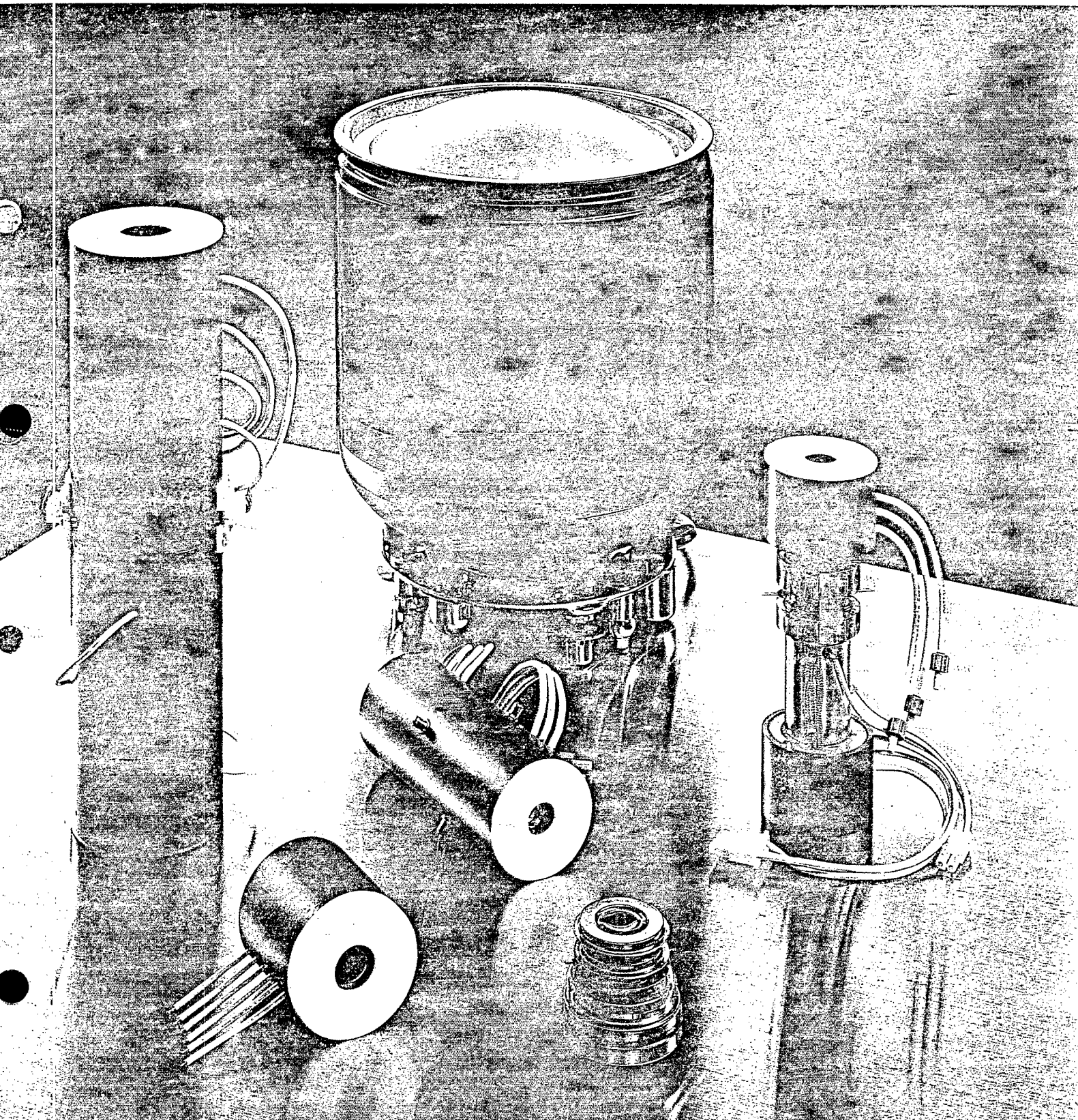

Terminology Used in This Catalog

Photocathode

A semi-transparent cathode which releases electrons when struck by light. Sensitivity to various wavelengths may be achieved by selecting the material used for the cathode surface and window.

Photocathode Sensitivity

Luminous: The photoelectric current from the photocathode per the incident light flux from a tungsten lamp at 2856 K. This is expressed in microamperes per lumen (μA/lm). This measure of sensitivity originally referred to light sensors for the visible light region.
Radiant: The photoelectric current from the photocathode per the power of the input monochromatic light. This is expressed in milliamperes per watt (mA/W) at a wavelength of interest.

Spectral Response

A photocathode's sensitivity varies depending upon the wavelength of the incident light; the spectral response is the relationship of photocathode sensitivity to wavelength.

Phosphor Screen

A screen made of a material which emits light when struck by X-rays, ultraviolet radiation or electrons.

Luminous Emittance

This is the measure of the density of the luminous flux emitting from a phosphor screen and is expressed in radolux (rlx) in the SI system or lumen/m^2. In addition, other units such as nits or foot Lambert (fL) are used, with conversions being made at 1 rlx = 0.318 nit or 0.0292 fL.

Illuminance

The density of the luminous flux on a surface (lm/m^2). 1lm/m^2 equals to 1 lx or 0.0929 fC.

Photon

The photon is a quantized particle of light which has the properties of both wave motion and particles simultaneously. Photons of a wavelength λ have an energy of hc/λ (h: Planck's constant, c: speed of light).

Photon Counting Method

This is the method of counting individual photons. When light strikes a photocathode, photoelectrons are emitted. For high-intensity light, the photocurrent is large and can be measured as an analog quantity. However, for extremely low-level-light, the interval between emissions of photoelectrons becomes large. Therefore, rather than measure the photoelectrons as a photocurrent, it is possible to obtain more accurate results by counting photons.

Particle Counting

Particle counting refers to the detection and counting of charged particles (electrons, beta-rays, positrons, alpha particles and related molecular ions) other than photons (visible light, ultraviolet to x-ray and gamma-rays). Although a photocathode is required to detect photons, direct detection for other particles, is possible using an MCP.

Picosecond

10^{-12} second. This is the time required for light to travel 0.3 mm in a vacuum. At present, it is the limit of man's current measurement and control capability.

Fiber Optic Plate

A plate consisting of bundles of parallel fibers which transmits light.

Microchannel Plate (MCP)

The MCP is an electron multiplier consisting of many bundled channels (micro glass capillaries) fused into the form of a thin plate. Each channel has a diameter of 10 to 20 μm and operates as an independent multiplier with a gain of approximately 10^4. Therefore, it can perform electron multiplication while retaining two-dimensional information.

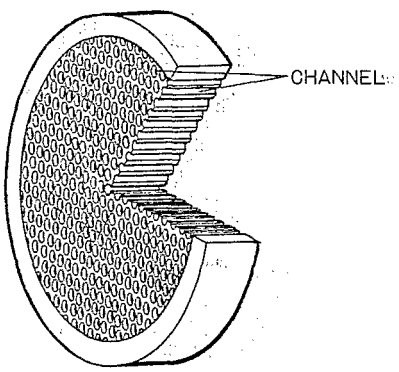

Schematic construction of MCP

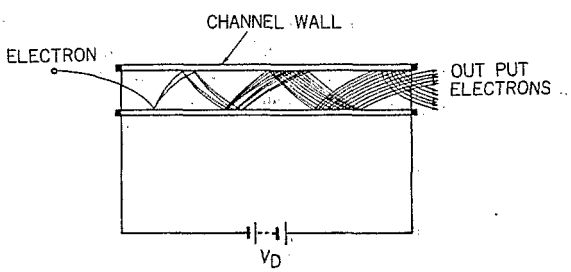

Operation of electron amplification

SIT Camera

A high sensitivity camera using a Silicon Intensifier Target (SIT) tube.

ISIT

Abbreviation for Intensifier Silicon Intensifier Target

Magnification

The image size produced on the phosphor screen divided by that focused on the photocathode. The average magnification on the tube axis is used to specify this parameter.

Thermionic Noise

This is the noise caused by thermionic emission from the photocathode surface. It can be minimized by cooling the photocathode.

S/N

This is the ratio of signal to noise.

MTF (Modulation Transfer Function)

In measuring resolution, as the stripe pattern density is increased, a limit is reached below which the contrast of the black-and-white stripe pattern having sinewave density variations cannot be lowered without making the pattern indiscernible.

The relationship between this contrast percentage and the number of line-pairs is referred to as the MTF. The MTF can be specified in percent at a particular number of line-pairs.

Limiting Resolution

The limiting resolution is a measure of the maximum ability to delineate picture detail. It is expressed as the maximum number of line-pairs per millimeter (lp/mm) that can be discerned when a black-and-white stripe pattern is focused on the photocathode. In this catalog, the value at MTF 5% is listed.

Spatial Resolution

Spatial resolution is defined as the minimum distance between two points or two lines on the spatial coordinates (at the photocathode surface) that may be separated. It is expressed as the FWHM of the output when a light point or line of infinitely small width is incident on the photocathode surface.

Dynamic Range

Dynamic range is the measure of the maximum span between the measured maximum and minimum signal levels achievable under linear input-output characteristics.

Radiant Emittance Gain

The ratio of the phosphor screen radiant emittance in watts per square meter (W/m^2) to the irradiance (W/m^2) on the photocathode. In this catalog, values apply for the input light of a wavelength at which the maximum photocathode sensitivity occurs and the output light emitted by a P-20 phosphor screen (peak wavelength: 550nm).

PSD (Position-Sensitive Detector)

The PSD consists of a resistive layer uniformly formed on the surface of a silicon photodiode and surrounded by signal output electrodes. When light or electrons strike this surface, an electric charge develops at the point of incidence. The charge is divided through the resistive layer and collected as a photocurrent by each electrode. Since the photocurrent is inversely proportional to the electrodes' distance from the point of incidence, the actual position can then be obtained by calculating these output signals.

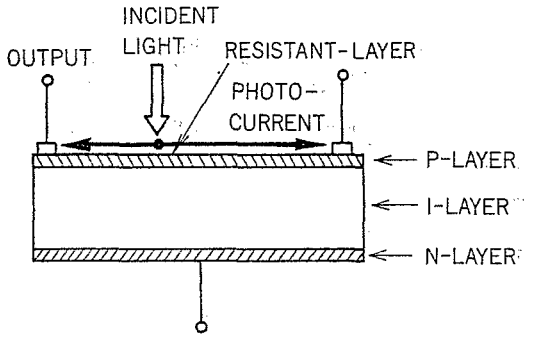

Electron Bombardment Effect

When electrons accelerated by an electric field bombard a semiconductor of silicon or other materials, the kinetic energy of the electrons causes the ionization of many atoms, resulting in the generation of free electrons. This is called the electron bombardment effect; in the case of a PSD, electrons accelerated by 3 kV will achieve an electron multiplication ratio of 100 or greater by this effect.

Electronic Cooling Element

This element uses the Peltier effect which describes the absorption and generation of heat when a current flows through a junction.

Pulse Height Distribution

The electron multiplication ratio of an MCP exhibits statistical variations manifest as a characteristic pulse height distribution. If a single-stage MCP is used without saturating the multiplication mechanism, this distribution is normally an exponential function. However, if a space charge causes saturation and this effect becomes dominant, the distribution will exhibit a peak. In addition, for 2- and 3-stage MCPs, this peak becomes pronounced and is easily separated from noise caused by dark current.

Dark Count

The dark count is the number of bright spots at the phosphor screen or the number of PSD signal pulses with zero incident light impinging on the photocathode under normal operating conditions. It is expressed as the count per second per mm^2 of photocathode area (cps/mm^2). This can be measured at either room temperature (25°C) or with refrigeration to −15°C.

PHOTON COUNTING IMAGERS

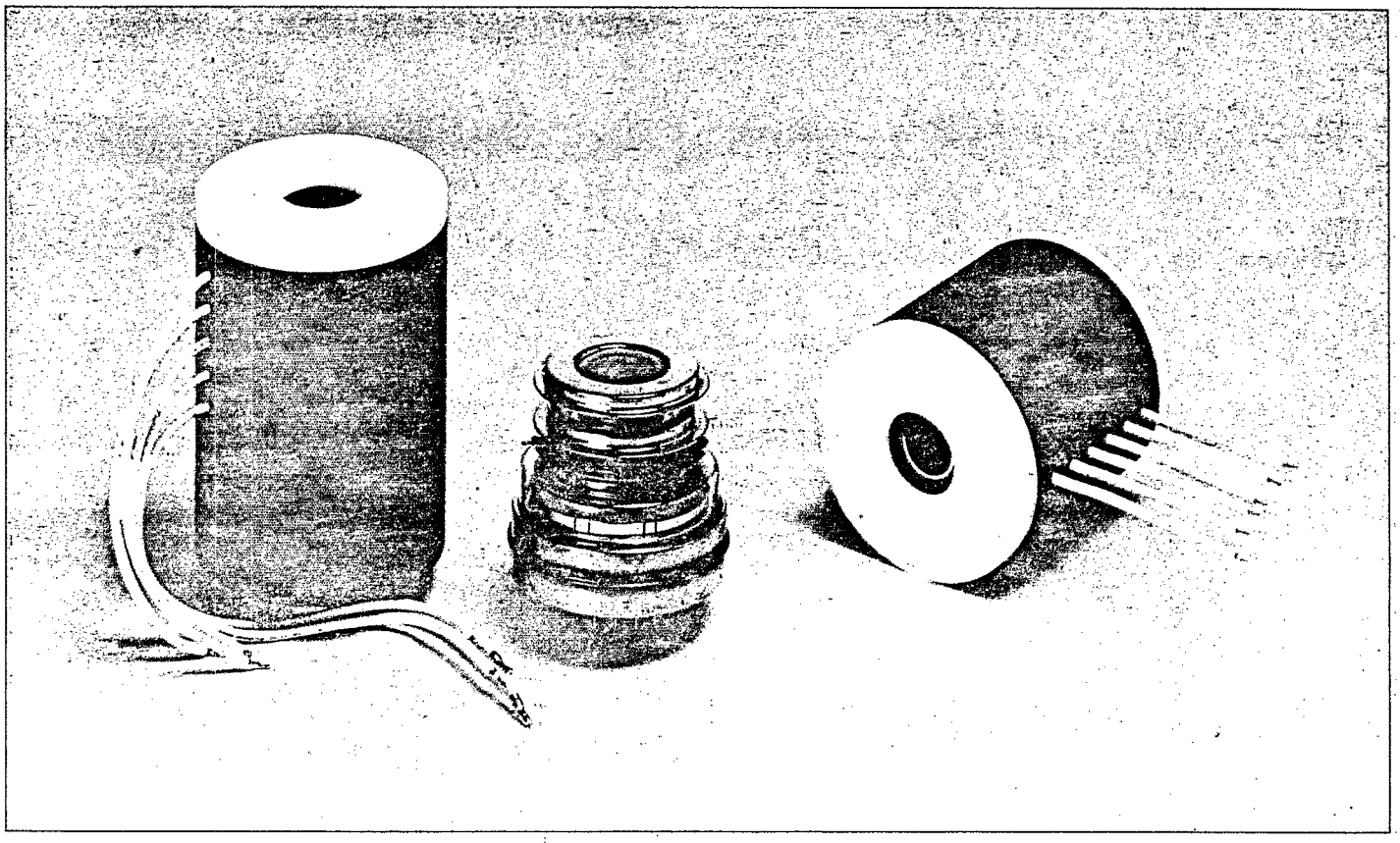

What is a Photon Counting Imager

Photon counting imagers are imaging tubes which use photon-counting technology to enable the measure of ultra-low level light. The photon counting level is of an intensity of 1/100,000 or even 1/1,000,000 of what a human would call "pitch black" (e.g. a night in the mountains with no moon). While SIT cameras, image intensifiers and similar devices are available to measure low level light, these devices are capable of obtaining images only in the above-mentioned "pitch blackness". Below this light level, further increases in the sensitivity of the imaging device do not result in images.

Photon counting imagers have been developed for imaging at such ultra-low light levels. Two types of Hamamatsu photon counting imagers are available; the phosphor screen output type and the PSD output type, these being selectable for individual application requirements.

Imaging at Ultra-Low Light Levels

At ultra-low light levels of light intensity, it becomes difficult to detect and measure the light as an analog quantity and the technique of detecting light as particles (photons) is more effective. However, the signal resulting from individual photons is extremely weak and it is not possible to obtain an image from the photon signal as is. At such ultra-low light levels, a common technique is the photon counting method using a photomultiplier tube. The light may be treated as a series of separate particles and each signal pulse detected by the photomultiplier tube represents each individual input photon. By counting these pulses, it is possible to quantitatively measure the light.

It should be remembered, however, that the photomultiplier tube is a point sensor and does not detect spatial information (i.e., from what part of the observed object light is emanating). The photon counting imager can be considered a two-dimensional photomultiplier tube capable of photon counting in two dimensions which provides position information on individual photons.

Figure 1-1 Imaging Devices for Various Ranges of Incident Light Level

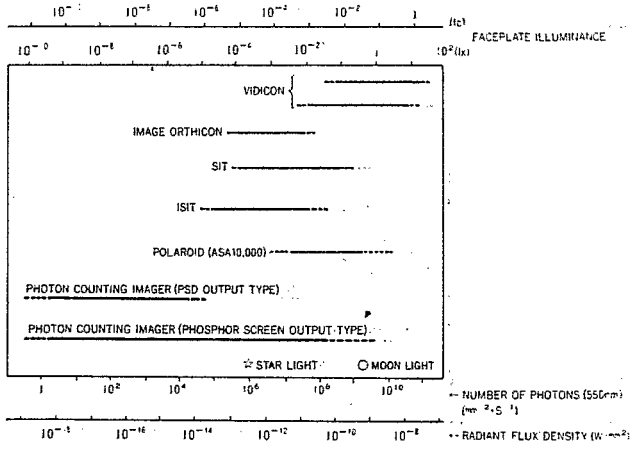

The detection limit of a photon counting imager is one to several tens of photons per 1mm^2. At 550 nm, this corresponds to 10^{-9} to 10^{-8} lux and 10^{-18} to 10^{-17}W/mm^2 radiated energy—an extremely low level of light.

Construction and Operation of Phosphor Screen Output Type

CONSTRUCTION

Figure 1-2 shows the construction of the V2025 photon counting imager. The V2025 consists of a photocathode, an electron lens, a two-stage MCP (microchannel plate) and a phosphor screen sealed in an evacuated glass envelope and potted with silicone rubber for protection. Its construction is similar to that of second-generation image intensifiers (with the exception of the use of a two-stage MCP) and, thus, may be termed an high sensitivity image intensifier. A flat input window is used and a fiber optic plate may be used for the window as well.

Figure 1-2 Phosphor Screen Output Type Construction

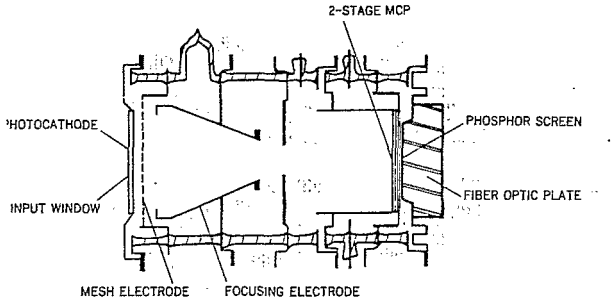

OPERATION

Figure 1-3 shows the operating principle of a phosphor screen output type photon counting imager. When an image is formed onto the photocathode by the lens, photoelectrons are emitted, depending upon the intensity of the light. They are focused onto the MCP as an electron image by the electron lens. The MCP is a two-dimensional electron multiplier at which one electron results in 10^2 to 10^3 secondary electrons. The multiplied electrons then impinge upon the phosphor screen by a high electric field where they are converted into a visible image.

The difference here with respect to a normal image intensifier is the ability to select one of two operating methods. One, used at intensities as low as 10^{-4} lx, is similar to that of an image intensifier which provides an output image with continuous tone of light level. In this type of operation, the multiplication ratio of the MCP is kept in the approximate range of 10^2 to 10^4 to prevent saturation. This type of operation is called analog mode operation.

The other mode of operation is used at extremely low level light of 10^{-5} lx and below. In this region, the incident light becomes a series of discrete particles (photons) and the resulting generated photoelectrons are of a level such that one only may enter each channel of the MCP. It is impossible to obtain a continuously toned image. For this reason, the MCP multiplication ratio is set at as high as 10^6 so that bright spots representing individual photoelectrons are generated on the phosphor screen. Since the MCP multiplication is saturated, these bright spots have uniform intensity. Under these conditions, the gradations of the output image intensity do not represent image intensity but rather temporal and spatial density to store the output image, enabling time storage of the incident light and reconstruction of an image. This mode of operation is called the photon counting mode.

Figure 1-3 Operating Principle of Phosphor Screen Output Type (V2025)

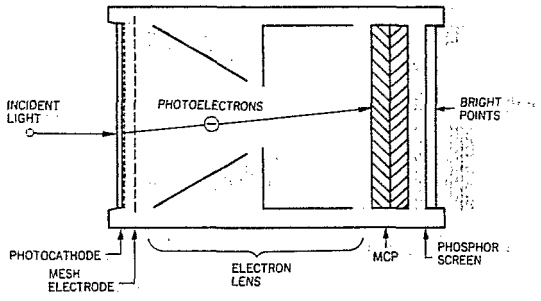

Figure 1-4 Two-Stage MCP Pulse Height Distribution

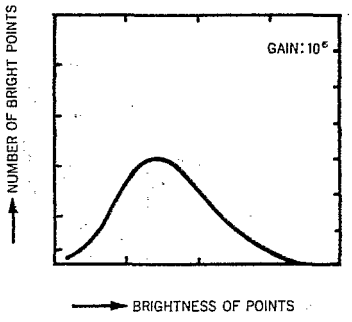

The ability to use the analog mode and the photon counting mode enables use over a very wide range of light intensities, spanning the ultra-low level region to the regions generally encountered in TV cameras. Switching between these modes is performed, as shown in Figure 1-5, when the photoelectron count per one mm^2/s is several hundred. Also, when using a phosphor screen output type photon counting imager in the photon counting mode as part of a system, the video signal is discriminated into two levels by digital processing as shown in Figure 1-6. The height (brightness) of the video signal of the single photon spots has no significance. It is important for creating the image to detect the position of bright spots. Therefore, the discriminator level is set at a point slightly above the video signal dark level to code the video signal into on and off (1 and 0) regions which is then transferred to a video frame memory.

Figure 1-5 Resolution vs. Number of Photoelectrons (Read out by a Saticon)

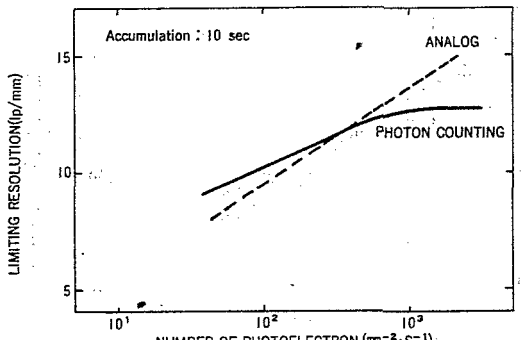

Figure 1-6 Photon Counting/Analog Mode Image Processing

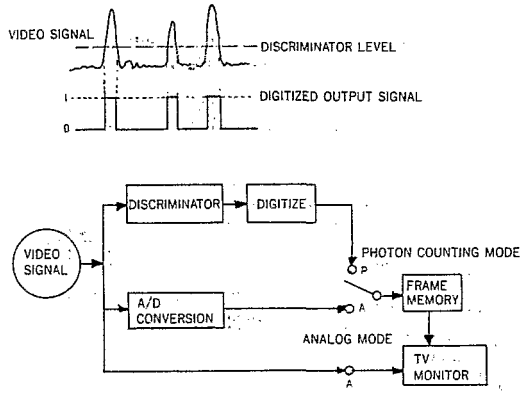

Construction and Operation of PSD Output Type

CONSTRUCTION

Figure 1-7 shows the construction of the N1831 PSD output type device. The device is potted with silicone rubber for protection and consists of a photocathode, electron lens and MCP—essentially the same as for the V2025 phosphor screen output type described above. However, a semiconductor PSD (position sensitive detector) that is incorporated instead of the phosphor screen. Also, a three-stage MCP is used to achieve a higher multiplication ratio. In addition to the flat input window, a fiber optic plate is also available.

Figure 1-7 PSD Output Type Construction

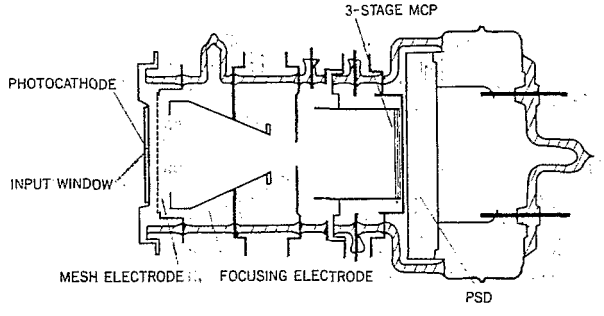

OPERATION

In contrast to the phosphor screen output type device; the PSD output type device can not be operated in the analog mode, therefore, it can not be used in an intensity region having a high number of photons. However, it provides an image of high resolution at extremely low light levels (refer to Figure 1-10).

When an image is formed onto the photocathode by a lens, photoelectrons are emitted from the surface, depending on the intensity of incident light. The emitted photoelectrons are lead to the MCP by the mesh electrode and the electron lens, and are multiplied by about 10^7 at the MCP. The multiplied electrons then bombard the PSD where they are multiplied further by approximately 100 and appear as an output current at the output terminals.

Figure 1-8 Operating Principle of PSD Output Type

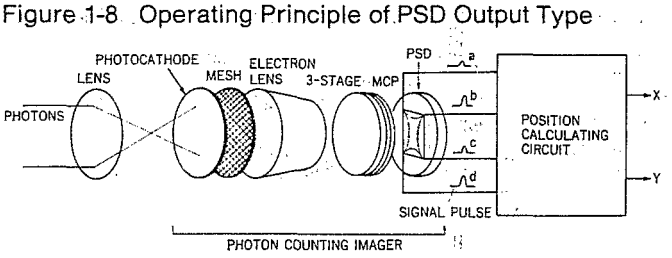

The operation of the PSD itself is quite different from that of the phosphor screen. The PSD is a type of large-area photodiode, and by connecting a processing circuit to this device, it is possible to obtain output signals representing the position of incidence of electrons or light on the surface of the device. The accuracy of position measurement is in the order of ±0.7% and the position resolution is 0.05%, both of these figures representing excellent performance. Essentially, each time a photoelectron is released from the photocathode, it is possible to obtain its accurate position signal from the PSD.

The position signals from the PSD output type device are input to an image processing unit which stores them to reconstruct the image. When a broadened electron group impinges upon the PSD, a signal is output which represents the center position of the group. While this eliminates the need to limit the incident electrons or light beam to a narrow spot, the simultaneous arrival of two or more such electron groups can result in an erroneous output signal. When this occurs, the current flowing is two times the normal current, so that the problem may be easily solved by eliminating output signals over a given current level. To achieve this, two discrimination levels are used, as shown in Figure 1-9, to form a window which enables only signals inside this range to be stored.

Figure 1-9 Window Gate

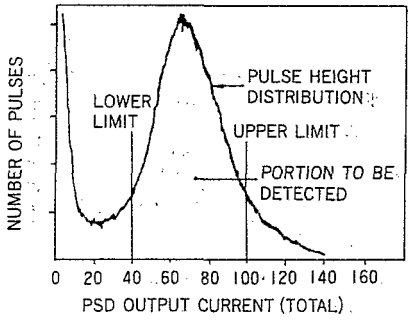

Figure 1-10 Spatial Resolution vs. Count

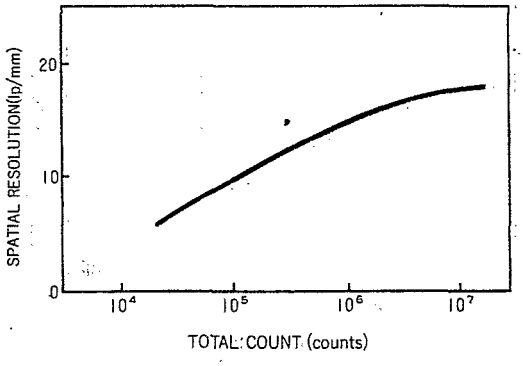

Characteristics of Photon Counting Imagers (Phosphor Screen Output Type)

Type No.	Features	Spectral Response		Photocathode			Phosphor Screen			Typical Supply Voltage ( ): maximum ratings		
		Range (nm)	Wavelength of Peak Response (nm)	Material	Effective Diameter Min. (mm)	Ⓐ Window Material /Thickness (mm)	Material	Effective Diameter Min. (mm)	Ⓐ Window Material /Thickness (mm)	Photocathode to Phosphor Voltage (kVdc)	Photocathode to Mesh Voltage (kVdc)	Mesh to MCP-In Voltage (kVdc)
V2025U	For visible light	280~650	420	Bialkali	15	B/1.5	P-20	15	F/10.0	6~6.9 (8)	0.5 (0.75)	0.5 (0.75)
V2025U-01	Near infrared extended version of V2025U	280~850	400	Multialkali	15	B/1.5	P-20	15	F/10.0	6~6.9 (8)	0.5 (0.75)	0.5 (0.75)
V2025U-02	Ultraviolet extended version of V2025U	180~650	420	Bialkali	15	U/1.5	P-20	15	F/10.0	6~6.9 (8)	0.5 (0.75)	0.5 (0.75)
V2025U-03	Ultraviolet-to-near infrared version of V2025U	180~850	400	Multialkali	15	U/1.5	P-20	15	F/10.0	6~6.9 (8)	0.5 (0.75)	0.5 (0.75)
V2025U-07	Fiber optic input type of V2025U	370~650	450	Bialkali	15	F/10.0	P-20	15	F/10.0	6~6.9 (8)	0.5 (0.75)	0.5 (0.75)
V2025U-08	Fiber optic input type of V2025U-01	370~850	470	Multialkali	15	F/10.0	P-20	15	F/10.0	6~6.9 (8)	0.5 (0.75)	0.5 (0.75)

※ Operating ambient temperature: −20 to +40°C, humidity: 40% or less

Ⓐ B: Borosilicate glass
J: UV glass
F: Fiber optic

Ⓑ Analog mode for MCP gain of 10^4 or below, photon couting mode forMCP gain of 10^5 to 10^6

Ⓒ Analog/photon counting mode

V2025U, -01, -02, -03

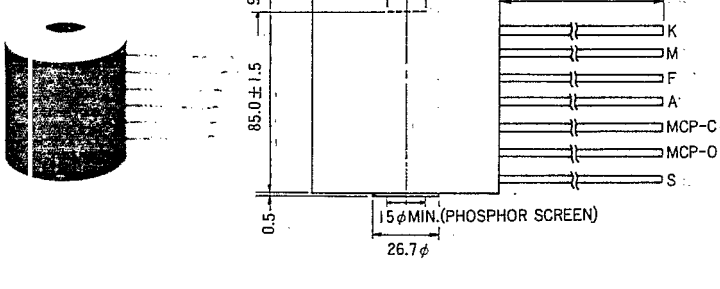

K: PHOTOCATHODE
M: MESH
F: FOCUSING ELECTRODE
A: ANODE
MCP-C: MCP-Center
MCP-O: MCP-Out
S: PHOSPHOR SCREEN

(Approx. 525g)

V2025U-07, -08

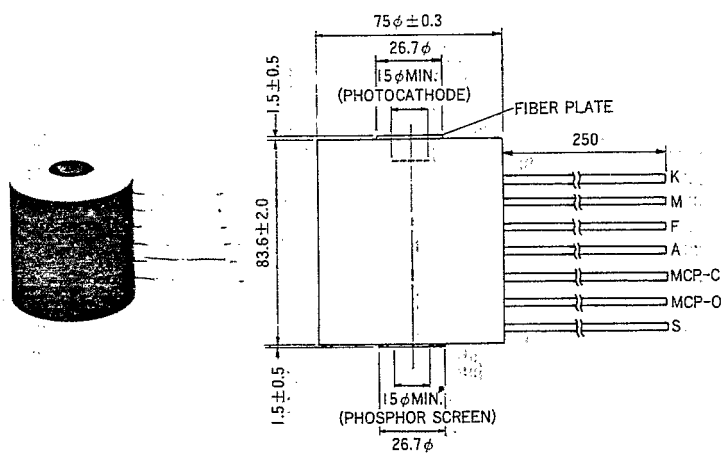

K: PHOTOCATHODE
M: MESH
F: FOCUSING ELECTRODE
A: ANODE
MCP-C: MCP-Center
MCP-O: MCP-Out
S: PHOSPHOR SCREEN

(Approx. 530g)

(at 25°C)

Typical Supply Voltage ( ): maximum ratings			Maximum Input Illuminance ❻		Photocathode Sensitivity				Luminous Emittance Max.	Limiting Resolution ❻ (Center) Typ.	Magnification Typ.	Dark Count Max.	Distortion Max.	Radiant Emittance Gain (MCP voltage: 1.9kV) (at 420nm)		Type No.
Photocathode to Focusing electrode Voltage (kVdc)	MCP Voltage (kVdc)	MCP-Out to phosphor Voltage (kVdc)	Analog mode (lx)	Photon Counting mode Photon/cm^2·s	Luminous (μA/lm)		Radiant (mA/W)									
					Min.	Typ.	Min.	Typ.	(rlx)	(lp/mm)		(cps/mm^2)	(%)	Min.	Typ.	
0.1~0.2 (0.5)	1.0~1.9 (2.0)	4 (4.5)	10	10^6	30	60	60 (420nm)	70 (420nm)	50	18/15	1	0.2	5	5×10^7	1×10^8	V2025U
0.1~0.2 (0.5)	1.0~1.9 (2.0)	4 (4.5)	10	10^6	100	150	0.3 (800nm)	2 (800nm)	50	18/15	1	0.5 (−15°C)	5	5×10^7	1×10^8	V2025U-01
0.1~0.2 (0.5)	1.0~1.9 (2.0)	4 (4.5)	10	10^6	30	60	15 (254nm)	30 (254nm)	50	18/15	1	0.2	5	5×10^7	1×10^8	V2025U-02
0.1~0.2 (0.5)	1.0~1.9 (2.0)	4 (4.5)	10	10^6	100	150	15 (254nm)	30 (254nm)	50	18/15	1	0.5 (−15°C)	5	5×10^7	1×10^8	V2025U-03
0.1~0.2 (0.5)	1.0~1.9 (2.0)	4 (4.5)	10	10^6	25	45	30 (450nm)	40 (450nm)	50	18/15	1	0.2	5	5×10^7	1×10^8	V2025U-07
0.1~0.2 (0.5)	1.0~1.9 (2.0)	4 (4.5)	10	10^6	70	120	0.3 (800nm)	2 (800nm)	50	18/15	1	0.5 (−15°C)	5	5×10^7	1×10^8	V2025U-08

- **Spectral Response**

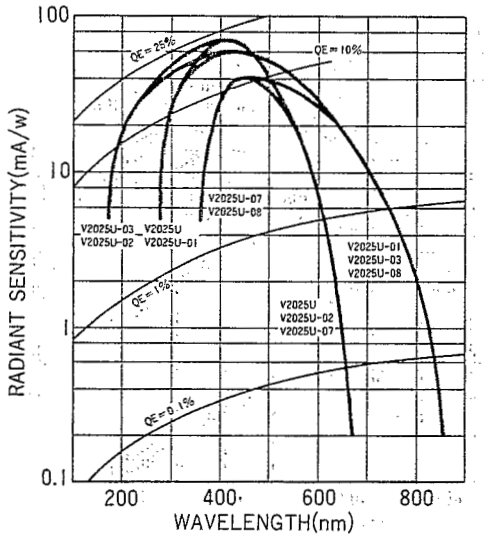

- **Phosphor Spectral Emission**

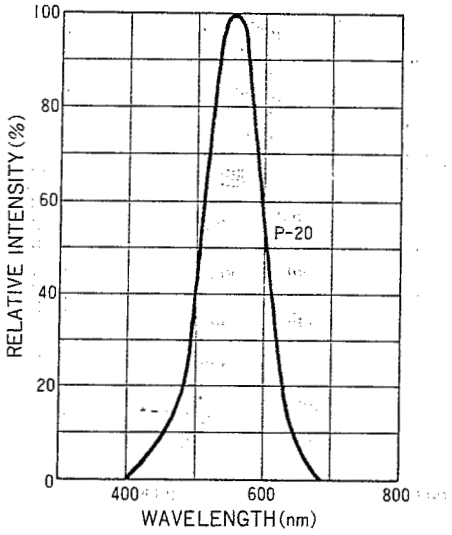

- **MTF (At Center)**

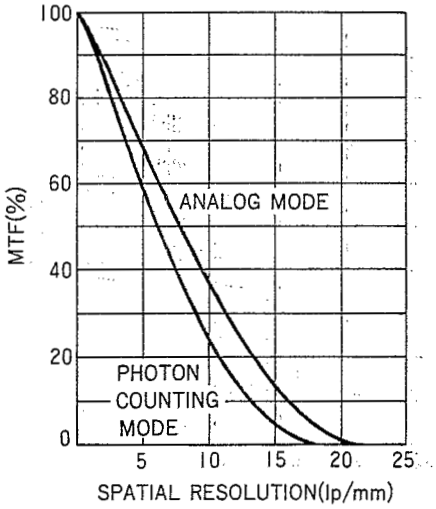

- **Phosphor Decay Characteristics (Typical Example)**

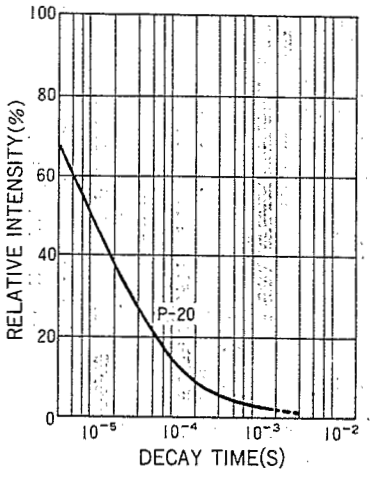

Characteristics of Photon Counting Imagers (PSD Output Type)

Type No.	Features	Spectral Response		Photocathode			Typical Supply Voltage ( ): maximum ratings			
		Range (nm)	Wavelength of Peak Response (nm)	Material	Effective Diameter Min. (mm)	Window Material /Thickness (mm) Ⓐ	Photo-cathode to PSD Voltage (kVdc)	Photo-cathode to Mesh (kVdc)	Mesh to MCP-In Voltage (kVdc)	Photocathode to Focusing electrode Voltage (kVdc)
N1831U	For visible light region	280~650	420	Bialkali	15	B/1.5	6.4 (8.5)	0.5 (0.75)	0.5 (0.75)	0.1~0.2 (0.5)
N1831U-01	Near-infrared extended version of N1831U	280~850	400	Multialkali	15	B/1.5	6.4 (8.5)	0.5 (0.75)	0.5 (0.75)	0.1~0.2 (0.5)
N1831U-02	Ultraviolet extended version of N1831U	180~650	420	Bialkali	15	U/1.5	6.4 (8.5)	0.5 (0.75)	0.5 (0.75)	0.1~0.2 (0.5)
N1831U-03	Ultraviolet-to-near infrared extended version of N1831U	180~850	400	Multialkali	15	U/1.5	6.4 (8.5)	0.5 (0.75)	0.5 (0.75)	0.1~0.2 (0.5)
N1831U-04	Ultraviolet version of N1831U	180~280	210	Cs-Te	15	U/1.5	6.4 (8.5)	0.5 (0.75)	0.5 (0.75)	0.1~0.2 (0.5)
N1718-01	For far ultraviolet (sapphire window)	145~195	160	Cs-I (MCP surface)	18	S/0.5	–	–	–	–
N1718-02	MgF_2 window version of N1718-01	115~195	140	Cs-I (MCP surface)	18	M/1.5	–	–	–	–

※ Operating ambient temperature: −20° to +40°C, humidity: 40% or less

Ⓐ B: Borosilicate glass
U: UV glass
S: Sapphire
M: MgF_2

Ⓑ Maximum counting rate, uniform over entire area with incident light at uniform time intervals (apporox. 1/10 of these figures for random input)

N1831U, -01, -02, -03, -04

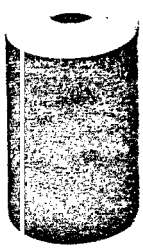

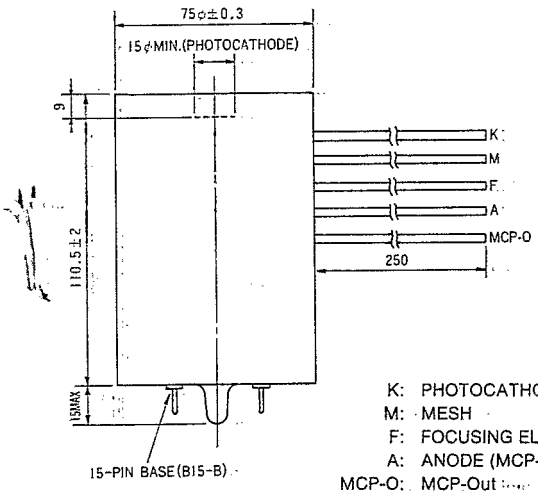

K: PHOTOCATHODE
M: MESH
F: FOCUSING ELECTRODE
A: ANODE (MCP-In)
MCP-O: MCP-Out

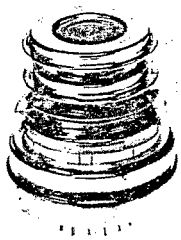

N1718-01, -02

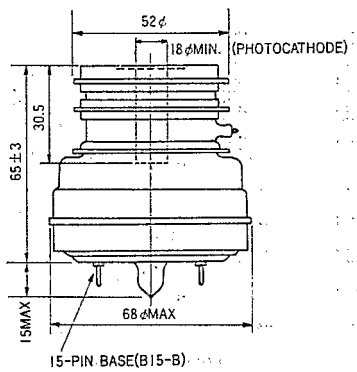

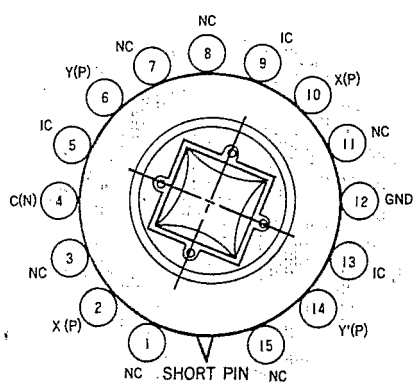

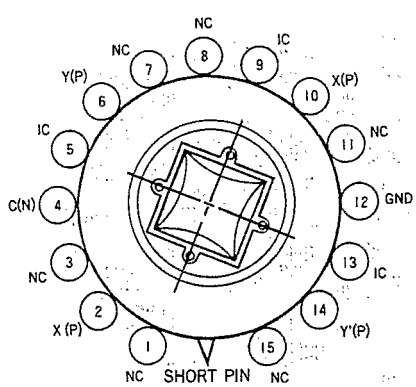

(at 25°C)

Typical Supply Voltage ( ): maximum ratings		Maximum Counting Rate	Photocathode Sensitivity				Limiting Resolution (Center) Typ.	Dark Count Max.	Distortion Max.	Gain		Weight	Type No.
MCP Voltage	MCP-Out to PSD Voltage		Luminous (μA/lm)		Radiant (mA/W)								
(kVdc)	(kVdc)	(cps)	Min.	Typ.	Min.	Typ.	(lp/mm)	(cps/mm^2)	(%)	Min.	Typ.	(g)	
2.4 (3.0)	3 (4)	2×10^5	30	60	60 (420nm)	70 (420nm)	18	0.6	3	10^7	10^9	500	N1831U
2.4 (3.0)	3 (4)	2×10^5	100	150	0.3 (800nm)	2 (800nm)	18	1.5 (−15°C)	3	10^7	10^9	500	N1831U-01
2.4 (3.0)	3 (4)	2×10^5	30	60	15 (254nm)	30 (254nm)	18	0.6	3	10^7	10^9	500	N1831U-02
2.4 (3.0)	3 (4)	2×10^5	100	150	15 (254nm)	30 (254nm)	18	1.5 (−15°C)	3	10^7	10^9	500	N1831U-03
2.4 (3.0)	3 (4)	2×10^5	–	–	15 (210nm)	20 (210nm)	18	0.1	3	10^7	10^9	500	N1831U-04
2.4 (3.0)	3 (4)	2×10^5	–	–	0.6 (160nm)	2.3 (160nm)	18	0.1	3	10^7	10^9	160	N1718-01
2.4 (3.0)	3 (4)	2×10^5	–	–	10 (125nm)	25 (125nm)	18	0.1	3	10^7	10^9	160	N1718-02

• Spectral Response

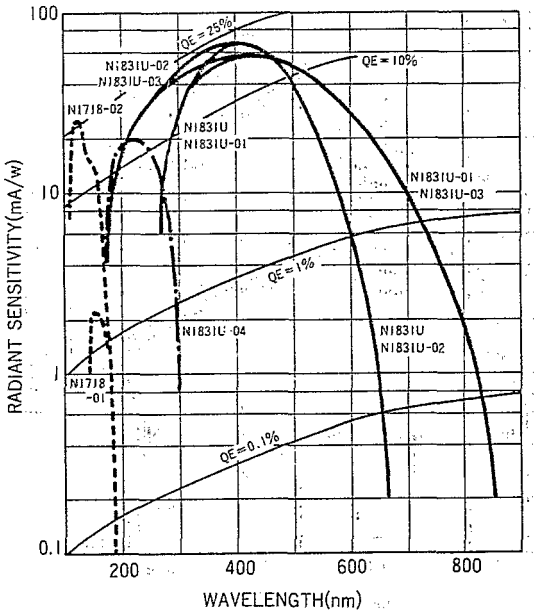

• Output Pulse Waveform

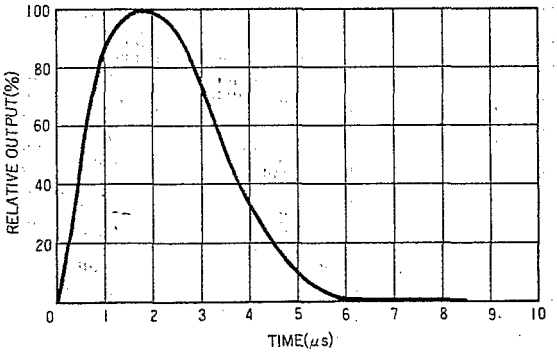

TEK INTEGRATED CIRCUITS OPERATION

CHARGE-COUPLED DEVICES
PRODUCTS AND SERVICES

SETTING THE PACE IN CCD TECHNOLOGY.

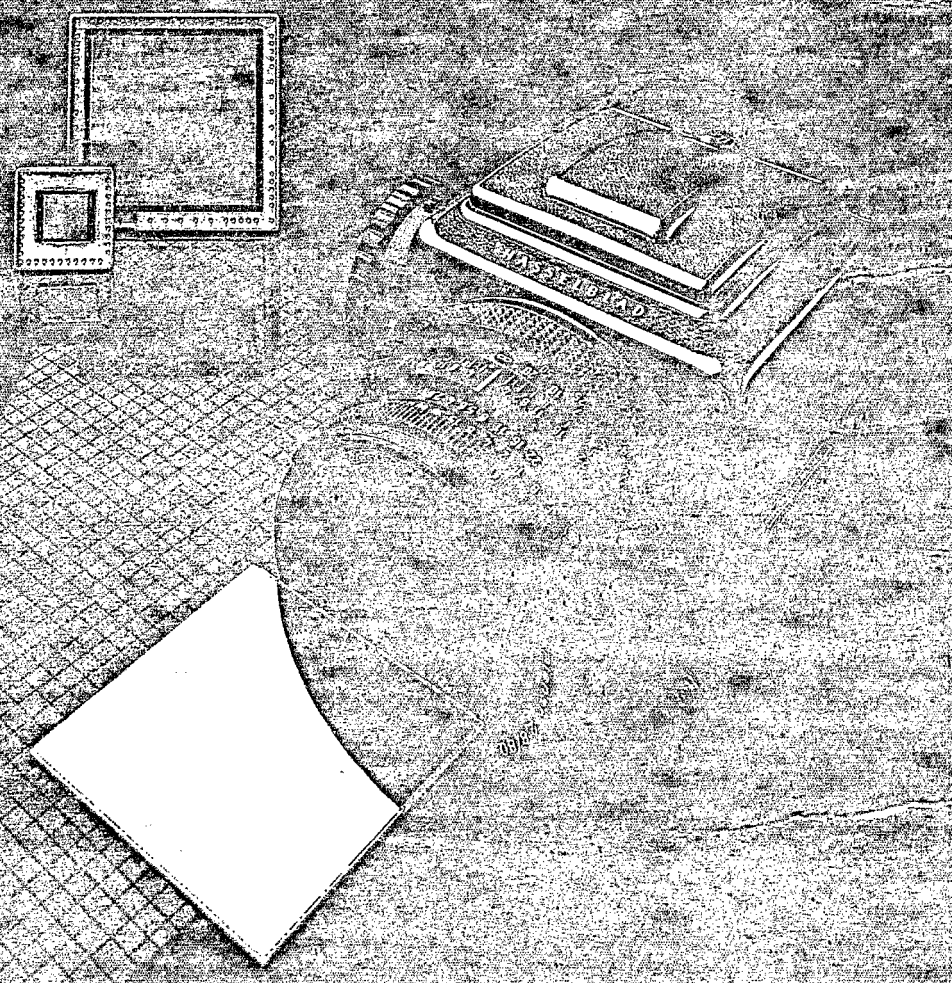

Tektronix
COMMITTED TO EXCELLENCE

BILL STEPHENS
Marketing Manager
CCD Products
Integrated Circuits Operation

Tektronix, Inc.
P.O. Box 500, Mail Sta. 59-420
Beaverton, OR 97077
Phone: 503-627-6101

Tektronix®
COMMITTED TO EXCELLENCE

KEY PARAMETERS TO CONSIDER WHEN COMPARING CCD IMAGERS FOR SCIENTIFIC APPLICATIONS

- Resolution – the number of picture elements (pixels) comprising the image.
- Read-out noise – the signal measured at the output in the absence of optical input. This, combined with quantum efficiency, and charge transfer efficiency determine the inherent device sensitivity, which is a measure of the minimal optical signal detectable with the imager.
- Quantum efficiency – the percentage of incoming incident light quanta, or photons, that generate electrons that are collected in a CCD pixel. This specification is wavelength dependent.
- Dark current – the rate at which charge generated in the device itself is injected into the CCD pixels in the absence of optical input. This is a function of temperature and processing parameters, and ultimately limits the sensitivity of the imager by limiting the integration time (or exposure time) of the device.
- Dynamic range – the ratio of peak signal carrying capacity of the device (based on linearity constraints) to a minimum output signal usually established by the readout noise capability of the device. For black and white imaging, this essentially specifies the number of intensity levels that can be resolved.
- Charge transfer efficiency (CTE) – a measure of completeness of charge transfer. It specifies the percentage of charge that is transferred during a clock transfer cycle. This is usually a function of signal level, and poor CTE can reduce dynamic range (and sensitivity) particularly at low signal levels.

Recommended Operating Conditions

Supply	Voltage Range (volts)
V_{DD}	20–30
Serial clocks	0–15
Parallel clocks	0–15
Reset Drain	12–15
Reset Gate	0–15
Input Diode	0–20
Sample Gate	0–15
Last Gate	0–4
Summing Well	0–15
V_{GG}	0–7
Transfer Gates	0–15
Source Supply, V_{SS}	≥0

Voltages are referenced to the backside contact.

Typical Device Specifications

	TK512M	TK2048M
Format	512 x 512 pixels Full Frame	2048 x 2048 pixels Full Frame
Process	Three phase Three level poly	Three phase Three level poly
Pixel Size	27µm x 27µm	27µm x 27µm
Imaging Area	13.8 x 13.8mm²	55.3 x 55.3mm²
Clocks	0–15 Volts	0–15 Volts
Dark Current at 25°C	10nA/cm²	10nA/cm²
Charge Transfer Efficiency (CTE)	.99999	.99999
Quantum Efficiency	50% at 700nm	50% at 700nm
Readout Noise T = –90°C Bandwidth–200kHz (See *figure 3*)	10e⁻ Amplifier A 20e⁻ Amplifier C	10e⁻ Amplifier A 20e⁻ Amplifier C
Full pixel signal— # electrons	700K	700K
Output amplifier gain (See *figure 3*)	Amplifier A–.5µV/e⁻ Amplifier C–2µV/e⁻	Amplifier A–.5µV/e⁻ Amplifier C–2µV/e⁻
Clock line capacitance	Φ_B–2500 pF $\Phi_{A\text{ or }C}$–200 pF	Φ_B–0.4µF $\Phi_{A\text{ or }C}$–800 pF

Functional Description:

The Tektronix CCD's are three phase three level polysilicon gate devices utilizing buried channel technology. *Figures 1A* and *1B* show a schematic outline of the TK512M and TK2048M devices.

The device is structured in a serial-parallel-serial (SPS) array and is intended for use as a full frame imager.

Imaging Area

The imaging area consists of a square array of 512 (or 2048) columns—each of which contains 512 (or 2048) CCD picture elements (pixels). Each pixel is 27µm x 27µm square and the columns are isolated from each other by 6µm channel-stop regions. The device is a buried channel structure designed to take advantage of the low dark current and high CTE inherent with this process. Three levels of polysilicon are used to fabricate the three gate electrodes which form the basic CCD cell. All of the pixels in a given row are defined by the same three gates. Corresponding gates in each of the pixels in a column are bussed in parallel at both edges of the chip. The signals used to drive this section are brought in from both edges of the array, thus speeding up the rate at which the columns can be clocked.

By maintaining one of the three electrical phases at a positive bias and the other two relatively low, potential wells form beneath the high gates. If an optical image is focused onto the array, an electronic analog of the scene will be collected in the potential wells.

The imaging section consists of 512 (or 2048) ϕ_1 and ϕ_3 gates and 513 (or 2049) ϕ_2 gates. (See *Figures 2A* and *2B*). Consequently, during integration if the ϕ_2 gates are held high (i.e., charge collected beneath these gates) there will be 513 (or 2049) lines of data. If either ϕ_1 or ϕ_3, or both are held high during the integration interval, the image will consist of 512 (or 2048) lines.

Following the integration interval the device may be read out as a normal full frame imager by transferring the collected charge one or more rows at a time into the serial (horizontal) shift register and then shifting that charge to the output. The transfer gate allows line summing into the serial register.

The device is designed such that imaging data can be bidirectionally read out; that is, charge packets may be clocked to either end of the image sensing area and transferred to either of the two output amplifiers, described below, located at opposite ends of the array. The *CCD Timing Diagram* (at right) defines typical timing and control signals, and two sets of clock designations. Assignment of these signals to the appropriate pins essentially selects the desired transfer direction. It should be noted however, that array data cannot be read-out through both amplifiers simultaneously.

Horizontal Registers

There are two serial (horizontal) shift registers on the chip; one at the top and one at the bottom of the imaging area. The registers are identical except for the output amplifiers as described in the next section. The registers each have 512 (or 2048) pixels plus a 50 pixel extension. Each register is provided with an input diode and a sampling gate in order to electrically inject a charge into the device (generally used only for testing purposes).

The output of the serial register is terminated in an output summing well, a DC biased gate (which serves to decouple the serial clock pulses from the output node), and the reset transistor. The well capacity of a pixel in the horizontal register is twice that of a parallel pixel.

Figures 2A and *2B* illustrate the detailed structure of the device. The figure shows how the gates in the imaging and horizontal registers are physically related. For example, the charge collected in the imaging section can be transferred to a ϕ_2 gate, through the transfer gate and then into a ϕ_3 gate of the C horizontal register.

The summing well is a separately clocked gate which has the well capacity of two serial pixels. Depending upon the specific application, this gate may be clocked with one of the normal serial clock phases or with its own pulse generator. The function of the summing well is to provide charge-summing of consecutive serial pixels, on chip, without adding any additional noise to the process.

Using the summing well it is possible to collect and detect the charge in small sub-arrays of the imaging section. This results in a loss of resolution, but is useful where low contrast, low signal-to-noise, diffuse scenes are being imaged.

Output Amplifiers

The imagers have two different output amplifiers. These are located at opposite corners of the device at the ends of the extended serial registers. *Figure 3* presents a schematic diagram of the two amplifiers. Both are floating-diffusion amplifiers.

The amplifier at the end of the A register is a simple, single stage MOSFET. This amplifier will require an off-chip load and is typically used in the source-follower mode.

In normal operation, a positive pulse is applied to the reset gate. This sets the potential of the floating diffusion to the potential applied to the reset drain. The reset gate voltage is then turned off and the output node (the floating diffusion) is isolated from the rest of the circuit. Charge from a serial pixel is then collected on the output node by sequencing the serial clocks through one cycle. The addition of charge on the output node is then sensed as a change in the voltage on the gate of the output MOSFET. This change in voltage is measured at V_{OA}.

The amplifier at the end of the C register operates fundamentally in the same manner. The difference between the two amplifiers is that the C amplifier is a dual source follower with on-chip self biased loads. Its sense transistor is a smaller device than the A amplifier, thus providing greater sensitivity (µV/electron). The output transistor of this amplifier is a very large device capable of driving a capacitively coupled 150 Ω load. The C amplifier is designed for high speed operation and has a design bandwidth in excess of 10 MHz.

In addition to the reset transistor, there are three required connections to the C amplifier. These are V_{DD}, V_{SS} and V_{OC}. The V_{SS} connection allows flexibility in biasing the low rail of this amplifier at some optimal voltage above the chip substrate. V_{OC} is the normal output and V_{DDC} is the drain supply.

Tektronix, Inc.
Tektronix Industrial Park
P.O. Box 500
Beaverton, Oregon 97077

Phone: (503) 627-7111
TWX: 910-467-8708
Telex: 151754

Tektronix
COMMITTED TO EXCELLENCE

PRICE LIST

CHARGE-COUPLED DEVICE IMAGERS

TEKTRONIX INTEGRATED CIRCUITS OPERATION

Effective date: 18 July 1985

Grade \ Device	TK512M -x1	TK512M -x2	TK2048M -x1	TK2048M -x2
GR 0	-	-	$52,000.00	$103,500.00
GR 1	$3450.00	$8050.00	$46,000.00	$92,000.00
GR 2	2875.00	6900.00	39,100.00	78,200.00
GR 3	2588.00	5750.00	28,750.00	57,500.00

NOTES:

NOMENCLATURE: Devices are designated as TKabcM-xy with the following code:

abc - model number designating pixel count
xy - x is grade (0,1,2,or 3); y is 1 for front-illuminated device, 2 for thinned back-illuminated device.

DISCOUNT SCHEDULE: (TK512M only)

QTY	Discount
10 - 24	10%
25 - 49	15%
50 - 99	20%
100 +	call ICO Marketing

QUALITY GRADES: The following grading system applies to imagers:
(x,y) - x is maximum no. of point defects
y is maximum no. of column defects

	TK512M	TK2048M
GR 0	-	(100,2) + extra output
GR 1	(10,0)	(100,2)
GR 2	(20,1)	(200,30)
GR 3	(40,3)	(400,100)